

# Light Curve Modeling of Superluminous Supernova 2006gy: Collision between Supernova Ejecta and Dense Circumstellar Medium

Takashi J. Moriya<sup>1,2,3\*</sup>, Sergei I. Blinnikov<sup>4,5,1</sup>, Nozomu Tominaga<sup>6,1</sup>, Naoki Yoshida<sup>7,1</sup>, Masaomi Tanaka<sup>8</sup>, Keiichi Maeda<sup>1</sup>, & Ken'ichi Nomoto<sup>1</sup>

<sup>1</sup> *Kavli Institute for the Physics and Mathematics of the Universe, Todai Institutes for Advanced Study, University of Tokyo, 5-1-5 Kashiwanoha, Kashiwa, Chiba 277-8583, Japan*

<sup>2</sup> *Department of Astronomy, Graduate School of Science, University of Tokyo, 7-3-1 Hongo, Bunkyo, Tokyo 113-0033, Japan*

<sup>3</sup> *Research Center for the Early Universe, Graduate School of Science, University of Tokyo, 7-3-1 Hongo, Bunkyo, Tokyo 113-0033, Japan*

<sup>4</sup> *Institute for Theoretical and Experimental Physics, Bolshaya Chermushkinskaya 25, 117218 Moscow, Russia*

<sup>5</sup> *Sternberg Astronomical Institute, Moscow University, Universitetski pr. 13, 119992 Moscow, Russia*

<sup>6</sup> *Department of Physics, Faculty of Science and Engineering, Konan University, 8-9-1 Okamoto, Kobe, Hyogo 658-8501, Japan*

<sup>7</sup> *Department of Physics, Graduate School of Science, University of Tokyo, 7-3-1 Hongo, Bunkyo, Tokyo 113-0033, Japan*

<sup>8</sup> *National Astronomical Observatory of Japan, 2-21-1 Ohsawa, Mitaka, Tokyo 181-8588, Japan*

18 August 2018

## ABSTRACT

We show model light curves of superluminous supernova 2006gy on the assumption that the supernova is powered by the collision of supernova ejecta and its dense circumstellar medium. The initial conditions are constructed based on the shock breakout condition, assuming that the circumstellar medium is dense enough to cause the shock breakout within it. We perform a set of numerical light curve calculations by using a one-dimensional multigroup radiation hydrodynamics code STELLA. We succeeded in reproducing the overall features of the early light curve of SN 2006gy with the circumstellar medium whose mass is about  $15 M_{\odot}$  (the average mass-loss rate  $\sim 0.1 M_{\odot} \text{ yr}^{-1}$ ). Thus, the progenitor of SN 2006gy is likely a very massive star. The density profile of the circumstellar medium is not well constrained by the light curve modeling only, but our modeling disfavors the circumstellar medium formed by steady mass loss. The ejecta mass is estimated to be comparable to or less than  $15 M_{\odot}$  and the explosion energy is expected to be more than  $4 \times 10^{51}$  erg. No  $^{56}\text{Ni}$  is required to explain the early light curve. We find that the multidimensional effect, e.g., the Rayleigh-Taylor instability, which is expected to take place in the cool dense shell between the supernova ejecta and the dense circumstellar medium, is important in understanding supernovae powered by the shock interaction. We also show the evolution of the optical and near-infrared model light curves of high-redshift superluminous supernovae. They can be potentially used to identify SN 2006gy-like superluminous supernovae in the future optical and near-infrared transient surveys.

**Key words:** supernovae: individual (SN 2006gy) — circumstellar matter — stars: mass-loss — early Universe

## 1 INTRODUCTION

Recent untargeted transient surveys such as Texas Supernova Search (Quimby 2006a), Palomar Transient Factory (Law et al. 2009; Rau et al. 2009), Catarina Real-time Transient Survey (Drake et al. 2009), Panoramic Survey Tele-

scope & Rapid Response System (Hodapp et al. 2004), discovered new kinds of supernovae (SNe). Among the most specutaclar are superluminous SNe (SLSNe) which become typically brighter than  $\sim -21$  mag in optical (e.g., Smith et al. 2007; Quimby et al. 2007, 2011; Rest et al. 2011; Miller et al. 2009; Gezari et al. 2009; Gal-Yam et al. 2009; Drake et al. 2010, 2011; Chatzopoulos et al. 2011;

\* takashi.moriya@ipmu.jp

Pastorello et al. 2010; Barbary et al. 2009; Chomiuk et al. 2011; Leloudas et al. 2012; Berger et al. 2012).

SN 2006gy is the first example of SLSNe with detailed photometric and spectroscopic observations. The luminosity of SN 2006gy stayed brighter than  $-21$  mag in the  $R$  band for more than 50 days (see Section 2 for a brief summary of observations). It was the most luminous SN ever reported at that time. Many theoretical models have been proposed to explain the huge luminosity of SN 2006gy. SN 2006gy was, at first, linked to Type Ia SNe exploding inside H-rich circumstellar medium (CSM) (e.g., SN 2002ic; Hamuy et al. 2003; Deng et al. 2004) (Ofek et al. 2007). However, the total observed radiation energy exceeded the available energy from a Type Ia explosion and thus the notion was abandoned.

Currently, SN 2006gy is thought to be caused by the death of a massive star. Several models have been proposed to explain the observed features as follows. All of them posit a massive progenitor star.

### (i) Large production of $^{56}\text{Ni}$

The energy released by the radioactive decay of  $^{56}\text{Ni}$  is a common luminosity source of SNe. However, more than  $10 M_{\odot}$  of  $^{56}\text{Ni}$  would be required to account for the peak luminosity of SN 2006gy (e.g., Nomoto et al. 2007). The large amount of  $^{56}\text{Ni}$  is not easily produced even by very high energetic core-collapse SNe (Umeda & Nomoto 2008). Pair-instability SNe (PISNe, e.g., Barkat, Rakavy, & Sack 1967; Rakavy & Shaviv 1967) can produce the large  $^{56}\text{Ni}$  but the rising time of SN 2006gy is found to be much shorter than that expected from a PISN (e.g., Kasen, Woosley, & Heger 2011; Nomoto et al. 2007; Moriya et al. 2010). The weakness of Fe lines in spectra at the late phase is also against the  $^{56}\text{Ni}$  heating scenario (Kawabata et al. 2009).

### (ii) Interaction between SN ejecta and dense CSM

The interaction between SN ejecta and dense CSM created by the progenitor before the explosion can make the luminosity of an SN very large. Strong shocks convert the kinetic energy of SN ejecta to thermal energy which is eventually released as radiation energy. Smith & McCray (2007) suggest that the declining phase of the light curve (LC) of SN 2006gy can be explained by emission from a shocked  $\sim 10 M_{\odot}$  CSM shell. Agnoletto et al. (2009) combined the  $^{56}\text{Ni}$  and shock interaction to explain the early LC of SN 2006gy. They argue that the rising part of LC is powered by  $^{56}\text{Ni}$  decay and the shock interaction comes into play from around the LC peak. Then, the required  $^{56}\text{Ni}$  mass is reduced to a few  $M_{\odot}$ .

### (iii) Pulsational pair-instability

Woosley, Blinnikov, & Heger (2007) relate SN 2006gy to the pulsational pair-instability. A very massive star with mass  $\simeq 80 - 130 M_{\odot}$  at the zero-age main sequence undergoes strong pulsations (see also Umeda & Nomoto 2008; Ohkubo et al. 2009), which induce the intermittent extensive mass loss. If the mass ejected by such an eruption is caught up by the mass released by the next eruption, the two massive shells collide and the star can eventually be as luminous as SN 2006gy. In this case, the luminosity source is the kinetic energy of the secondly ejected materials. Hence, the radiation mechanism is essentially the same as that of (ii) the interaction between SN ejecta and dense CSM. The ejecta from inside is released by the pulsational pair-instability,

rather than an SN explosion in this case. This kind of luminous transients are called pulsational pair-instability SNe.

### (iv) Spin-down of newly born magnetars

If a magnetar born at the time of the core collapse of a massive star has suitable magnetic field and spin, it can release its rotational energy efficiently just after the SN explosion. If the radiation energy released at the magnetar can be converted to thermal energy, SN ejecta surrounding the magnetar is heated up and the SN can become very bright (Kasen & Bildsten 2010; Woosley 2010, see also Maeda et al. 2007).

### (v) Transition of a neutron star to a quark star

Neutron in a neutron star formed at the core collapse can be further decomposed to quarks and they can form a quark star. When a neutron transforms to quarks, latent heat due to the phase transition can heat up the SN ejecta surrounding the quark star and make an SLSN (e.g., Leahy & Ouyed 2008; Ouyed et al. 2012; Kostka et al. 2012, see also Benvenuto & Lugones 1999).

Among the possible heating sources, the CSM interaction (ii and iii) is plausible because the spectra of SN 2006gy show narrow P-Cygni profiles that indicate the existence of a CSM outflow with  $\sim 100 \text{ km s}^{-1}$ . Although the observed low X-ray flux of SN 2006gy (see Section 2) might appear to contradict the interaction scenario, the CSM could be optically thick enough to absorb X-rays from the shock wave, or the shock wave itself could be cool (e.g., Blinnikov 2008; Chevalier & Irwin 2012; Svirski, Nakar, & Sari 2012).

Although the scenario (ii), i.e., the shock interaction between SN ejecta and dense CSM, is suggested to be able to explain the early LC of SN 2006gy, detailed LC models have not been explored yet. Chevalier & Irwin (2011); Moriya & Tominaga (2012); Svirski, Nakar, & Sari (2012) investigate the possibility of explaining SN 2006gy by the interaction of SN ejecta and dense CSM alone. They assume that the CSM is optically thick enough to cause the shock breakout within it (e.g., Weaver 1976; Nakar & Sari 2010, see also Ofek et al. 2010; Balberg & Loeb 2011 about the shock breakout in dense CSM). Chatzopoulos, Wheeler, & Vinko (2012) show the bolometric LC from the interaction scenario based on their semi-analytic LC model (see Section 6.4). The previous works regarding the collision of SN ejecta and dense CSM so far analyse the LC of SN 2006gy based on analytic approaches with several simplifications. The detailed numerical modeling of the LC of SN 2006gy has not been done yet and it is clearly required (see also the very recent attempt by Ginzburg & Balberg 2012).

In this paper, we study model LCs for SN 2006gy by using numerical radiation hydrodynamics code *STELLA*. Our purpose of the modeling is to show numerically that the simple analytic shock breakout model actually works well to explain overall features of the early LC of SLSN 2006gy. We focus on SN 2006gy because it is the best observed SLSNe currently reported. We do not aim at the perfect fitting of the LC because it does not necessarily lead us to the correct physical parameters of SN 2006gy. This is because *STELLA* makes several simplifications to numerically treat the radiation hydrodynamics. We rather concentrate on the overall features of the LC of SN 2006gy and show that the dense CSM configurations predicted by the shock breakout

model are actually working well to reconstruct the LC of SN 2006gy.

The rest of the paper is organized as follows. Section 2 is a short summary of the observations of SN 2006gy. In Section 3, **STELLA**, which is used for our LC modeling, is summarized briefly. How multidimensional effect is included in one-dimensional code **STELLA** is also overviewed in Section 3. Our models are introduced in Section 4 and the LC calculations based on the models are shown in Section 5. Discussion is given in Section 6. We close the paper with conclusions in Section 7. We use the standard cosmology with  $H_0 = 70 \text{ km s}^{-1} \text{ Mpc}^{-1}$ ,  $\Omega_M = 0.3$ , and  $\Omega_\Lambda = 0.7$  when it is required.

## 2 BRIEF SUMMARY OF OBSERVATIONS

We briefly summarize the observational properties of SN 2006gy. SN 2006gy was discovered by Texas Supernova Search on September 18, 2006 (UT) near the nucleus of an early-type galaxy NGC 1260 (Quimby 2006b). There are several suggested values for the extinction by the host galaxy (Ofek et al. 2007; Smith et al. 2007; Agnoletto et al. 2009). We adopt  $E(B - V)_{\text{host}} = 0.40$  mag following Agnoletto et al. (2009) with the Milky Way extinction  $E(B - V)_{\text{MW}} = 0.16$  mag (Schlegel, Finkbeiner, & Davis 1998). Thus, the total extinction is  $E(B - V) = 0.56$  mag or  $A_R = 1.3$  mag with  $R_V = 3.1$  (Cardelli, Clayton, & Mathis 1989). The distance modulus  $\mu$  of the host galaxy is also taken from Agnoletto et al. (2009) ( $\mu = 34.53$  mag).

Follow up spectral observations classified SN 2006gy as Type II<sub>n</sub> because of the narrow H emission lines presented in the spectra (see Schlegel 1990; Filippenko 1997, for the details of Type II<sub>n</sub>). The luminosity of SN 2006gy kept rising until October 25, 2006 (UT) and the peak *R* band luminosity got close to  $\simeq -22$  mag. The rising time is estimated as about 70 days (hereafter, days are in the rest frame). After reaching the peak luminosity, the LC declined slowly ( $\simeq 0.02 \text{ mag day}^{-1}$ ) for  $\simeq 120$  days and then the LC stayed almost constant for  $\simeq 20$  days until SN 2006gy hid behind the Sun. Near-infrared (NIR) LCs in these early epochs are consistent with the blackbody temperature obtained from the optical spectra and no significant excess was detected (Miller et al. 2010). No X-ray was detected when the LC is rising (Ofek et al. 2007) but weak X-rays may have been detected during the declining phase (Smith et al. 2007). No radio emission is detected at any observed epochs (Ofek et al. 2007; Chandra, Chakraborti, & Ray 2007; Argo et al. 2007; Bietenholz & Bartel 2007, 2008a,b).

Optical spectra of the early epochs are also taken intensively (e.g., Smith et al. 2010; Agnoletto et al. 2009). Spectra taken before the LC peak are characterized by Lorentzian H $\alpha$  emission lines (Smith et al. 2010). The origin of the Lorentzian profile is related to the existence of optically thick CSM (e.g., Chugai 2001; Dessart et al. 2009). Except for the narrow H emission lines, the spectra are featureless and characterized by blackbody with depletion in blue (Smith et al. 2010; Agnoletto et al. 2009). The reason for the lack of features may be partly because the spectra before the LC peak were taken only with low resolutions. After the LC peak, overall H $\alpha$  line profiles can be fitted by two Gaussian components with the FWHM of  $1,800 \text{ km s}^{-1}$  and

$5,200 \text{ km s}^{-1}$  and they are presumed to come from the interacting region between the ejecta and dense CSM (e.g., Smith et al. 2010). There also exists a broad absorption in the blue part of the H $\alpha$  profile which is suggested to originate from the ejecta inside. In addition, the spectra of SN 2006gy show narrow P-Cygni profiles from several elements (e.g., H, Fe) with the outflowing velocity  $\sim 100 \text{ km s}^{-1}$ . As the velocity is too slow to attribute it to the ejecta inside, those narrow lines are presumed to originate from the unshocked CSM. The strengths of these narrow lines decline with time and they are barely seen in the spectrum taken at  $\simeq 140$  days since the LC peak (Smith et al. 2010).

About 100 days later, SN 2006gy came out of the Sun and was observed again (Agnoletto et al. 2009; Kawabata et al. 2009; Miller et al. 2010). The optical luminosity of SN 2006gy declined dramatically (about 2 mag in the *R* band) which was almost constant for  $\simeq 20$  days before the SN went behind the Sun. The luminosity declined very slowly ( $\simeq 0.002 \text{ mag day}^{-1}$ ) since it appeared from the Sun for more than 400 days until the last reported observation on November 22, 2008 (UT) (Kawabata et al. 2009; Miller et al. 2010). The decline rate is much slower than that of  $^{56}\text{Co}$  decay ( $0.01 \text{ mag day}^{-1}$ ) and the main source of the luminosity cannot be the  $^{56}\text{Co}$  decay. Because of the high NIR luminosities, Smith et al. (2008); Miller et al. (2010) suggest that the late time luminosity is due to light echoes. The optical spectra of those epochs are dominated by intermediate width emission lines ( $\simeq 2,000 \text{ km s}^{-1}$ , Kawabata et al. 2009). H emission lines were weaker than those observed in previous epochs and suggest that the interaction is weak in those epochs and it is no longer a main source of the radiation (Agnoletto et al. 2009; Kawabata et al. 2009). Weakness of Fe lines in those epochs seems inconsistent with the large  $^{56}\text{Ni}$  production (Kawabata et al. 2009).

## 3 NUMERICAL METHOD

We briefly summarise the basics of **STELLA** code, which we use for our LC modeling. We then describe in detail a key numerical method of **STELLA** that treats smearing due to multidimensional effect.

### 3.1 STELLA

**STELLA** is a one-dimensional multigroup radiation hydrodynamics code (e.g., Blinnikov & Bartunov 1993; Blinnikov et al. 1998, 2006; Blinnikov & Tolstov 2011) and calculates the spectral energy distributions (SEDs) at each time step. Multicolor LCs can be obtained by convolving filter functions to the SEDs. All the calculations are performed by adopting 100 frequency bins from  $1 \text{ \AA}$  to  $5 \times 10^4 \text{ \AA}$  in log scale. **STELLA** implicitly treats time-dependent equations of the angular moments of intensity averaged over a frequency bin. Local thermodynamic equilibrium is assumed to determine the ionization levels of materials. **STELLA** has been intensively used for modeling the SN LCs powered by the shock interaction (e.g., Chugai et al. 2004; Woosley, Blinnikov, & Heger 2007; Blinnikov & Sorokina 2010; Moriya et al. 2011) as well as other types of SNe (e.g., Baklanov, Blinnikov, & Pavlyuk 2005; Folatelli et al. 2006;

Tsvetkov et al. 2009; Tominaga et al. 2011). Comparisons of STELLA with other numerical codes are provided in, e.g., Blinnikov et al. (1998, 2000, 2003); Woosley et al. (2007) and analytical models are also compared to the numerical results of STELLA (e.g., Rabinak & Waxman 2011).

### 3.2 Smearing

As is shown in the previous works (e.g., Chevalier & Fransson 1994; Chugai 2001; Chugai et al. 2004) and will be shown in the following sections, the interaction of SN ejecta and dense CSM results in a dense cool shell between SN ejecta and dense CSM. This is because of the radiative cooling of the shocked region. The shocked region becomes very dense and cools down efficiently by radiation. The cooling prevents the pressure from growing sufficiently enough to sustain the shell. Hence, the shell becomes thinner and denser and the cooling becomes more efficient. Thus, this cooling process is catastrophic. However, in reality, such a shell is unstable because of several instabilities like the Rayleigh-Taylor instability which require multidimensional calculations to treat (e.g., Chevalier & Blondin 1995). The multidimensional effect smears the shell and less kinetic energy is converted to radiation energy. In other words, the cooling by radiation is less efficient in three dimensions than in one dimension. In STELLA code, we take such multidimensional effects into account by introducing a smearing term in the equation of motion so that the conversion efficiency from kinetic energy to radiation energy can be reduced (Blinnikov et al. 1998). This term is similar to artificial viscosity, although the smearing term has completely opposite effect.

As is shown in Blinnikov et al. (1998), the smearing term is defined such that the total energy is manifestly conserved. Only the neighbouring zones are affected by the smearing term. The overall normalization factor  $R_{\text{cut}}(\tau)$  of the smearing is expressed as

$$R_{\text{cut}}(\tau) = B_q f(\tau). \quad (1)$$

See Blinnikov et al. (1998) for the definitions of  $R_{\text{cut}}(\tau)$  and the smearing term.  $f(\tau)$  is introduced so that the artificial smearing is reduced at optically thick regions where the effect of cooling is less efficient and the multidimensional instabilities due to the cooling grow less. In STELLA code,  $f(\tau)$  is an empirically obtained monotonically decreasing function which satisfies  $f(\tau \rightarrow 0) = 1$ .  $B_q$  determines the overall strength of the smearing effect. Ideally,  $B_q$  should be calibrated by comparing results obtained by our one-dimensional calculations to those of multidimensional calculations in which the effect of multidimensional instabilities in the shell are taken into account. However, such a multidimensional radiation hydrodynamical code with which we can compare our results is not available yet. We use  $B_q = 1$  as our standard value. We also show the effect of  $B_q$  on model LCs (Section 5.2.4 and Appendix A). The results of LC calculations strongly depend on  $B_q$ , as the smearing term directly affects the conversion efficiency from kinetic energy to radiation. We need a multidimensional radiation hydrodynamics code for the calibration of the parameter  $B_q$ .

## 4 INITIAL CONDITIONS

In this section, we show how the initial conditions for our LC calculations are constructed. Two components exist in the initial conditions: SN ejecta inside and CSM outside. We assume that there is a gap between the progenitor and the dense CSM. Then, it takes some time for the SN ejecta to reach the dense CSM and start to collide. We assume that the SN ejecta freely expands in the gap before the collision. We numerically follow the LCs after the collision. The initial conditions of the two components, SN ejecta and dense CSM, are constructed by the way explained in this section. Then, these initial conditions will be confirmed by our numerical LC calculations as we show in the later sections. The initial density structures of two representative models are shown in Figure 1 as examples. Both SN ejecta and CSM are assumed to have solar metallicity and no  $^{56}\text{Ni}$  is included in our calculations unless it is otherwise mentioned. The summary of the models is given in Table 1.

### 4.1 Supernova Ejecta

SN ejecta before the collision is assumed to be freely expanding with a homologous velocity profile. The analytic approximation for the density structure of SN ejecta provided by, e.g., Chevalier & Soker (1989) is adopted:

$$\rho(r, t) = \begin{cases} \zeta_\rho \frac{M_{\text{ej}}}{v_t^3 t^3} \left(\frac{r}{v_t t}\right)^{-\delta} & (v < v_t), \\ \zeta_\rho \frac{M_{\text{ej}}}{v_t^3 t^3} \left(\frac{r}{v_t t}\right)^{-n} & (v > v_t), \end{cases} \quad (2)$$

where  $M_{\text{ej}}$  is the SN ejecta mass,  $t$  is time since the explosion,  $v_t = \zeta_v (E_{\text{ej}}/M_{\text{ej}})^{1/2}$ , and  $E_{\text{ej}}$  is the kinetic energy of the SN ejecta. The constants  $\zeta_\rho$  and  $\zeta_v$  are constrained by the condition that the sum of density and kinetic energy should be  $M_{\text{ej}}$  and  $E_{\text{ej}}$ :

$$\zeta_v = \left[ \frac{2(5-\delta)(n-5)}{(3-\delta)(n-3)} \right]^{1/2}, \quad (3)$$

$$\zeta_\rho = \frac{1}{4\pi} \frac{(n-3)(3-\delta)}{n-\delta}. \quad (4)$$

In this paper, we adopt  $\delta = 1$  and  $n = 7$ , which is used by Chevalier & Irwin (2011). We have also tried  $n = 6$  and  $n = 8$  for some models but results had little difference compared to those of  $n = 7$ . The maximum velocity of the SN ejecta before the interaction is chosen to be high enough, so that most of the assumed  $E_{\text{ej}}$  is contained in the SN ejecta. It is around 20,000 – 50,000 km s<sup>-1</sup>.

$M_{\text{ej}}$  is difficult to be constrained only by the observations of the LC of SN 2006gy because the LC is mainly affected by CSM as is shown in the following sections. In most of the models, we adopt  $M_{\text{ej}} = 20 M_\odot$  because the progenitors of Type IIIn SNe are presumed to be originated from relatively massive stars. Effect of  $M_{\text{ej}}$  on LCs is discussed in Sections 5.2.3 and 6.1.

### 4.2 Circumstellar Medium

Dense CSM in the calculations is assumed to exist from  $R_i$  to  $R_o$  from the center and have a density structure  $\rho \propto r^{-w}$ .

**Table 1.** List of LC models

Name	$v_s$ km s <sup>-1</sup>	$M_{\text{ej}}$ $M_{\odot}$	$E_{\text{ej}}$ 10 <sup>51</sup> erg	$w$	$R_o$ 10 <sup>15</sup> cm	$y_1 R_o$ 10 <sup>15</sup> cm	$xR_o$ 10 <sup>15</sup> cm	$R_i$ 10 <sup>15</sup> cm	$M_{\text{CSM}}$ $M_{\odot}$	$\langle \dot{M} \rangle^a$ $M_{\odot} \text{ yr}^{-1}$	$B_q$
A1	5,200	20	50	5	11	4.9	1.8	1.0	22	0.70	1
A2	5,200	20	50	5	11	4.9	1.8	1.5	10	0.33	1
B1	5,200	20	10	2	8.8	3.3	0.090	0.090	0.83	0.030	1
B2	5,200	20	30	2	8.8	8.3	2.0	0.090	27	0.98	1
C1	5,200	20	50	0	4.9	4.8	1.8	1.0	14	1.1	1
D1	10,000	20	10	5	21	11	4.6	4.5	22	0.42	1
D2	10,000	20	10	5	21	11	4.6	5.0	18	0.36	1
E1	10,000	20	30	2	17	6.3	0.32	0.10	3.2	0.060	1
E2	10,000	2	10	2	17	6.3	0.32	0.10	3.2	0.060	1
F1	10,000	20	10	0	11	11	4.6	5.0	15	0.45	1
D3	10,000	10	10	5	21	11	4.6	5.0	18	0.36	1
D4	10,000	30	10	5	21	11	4.6	5.0	18	0.36	1
D5	10,000	10	5	5	21	11	4.6	5.0	18	0.36	1
D6	10,000	20	10	5	21	11	4.6	5.0	18	0.36	0.33
D7	10,000	20	10	5	21	11	4.6	5.0	18	0.36	3

<sup>a</sup> Average mass-loss rate.  $\langle \dot{M} \rangle = v_w M_{\text{CSM}} / (R_o - R_i)$  where  $v_w = 100 \text{ km s}^{-1}$  is the assumed CSM velocity.

The outflowing velocity of the CSM is  $100 \text{ km s}^{-1}$ . It is estimated from the narrow P-Cygni profile of H $\alpha$  appeared in the spectra of SN 2006gy (e.g., Smith et al. 2010). The CSM is assumed to be optically thick enough to cause the shock breakout within it. We estimate the physical conditions of the CSM from the observations by using the shock breakout condition described in Moriya & Tominaga (2012). Our main purpose of this paper is to see how well the properties of the dense CSM predicted by this simple shock breakout model in CSM can explain the overall LC features of SN 2006gy. We use following three values which can be estimated from the observations to derive the CSM properties: the photon diffusion time  $t_d$  in CSM, the propagation time  $t_s$  of the forward shock through CSM, and the forward shock velocity  $v_s$ .  $t_d$  corresponds to the rising time of the LC and  $t_s$  corresponds to the time when the narrow P-Cygni H $\alpha$  profiles from CSM disappears. We adopt  $t_d = 70$  days and  $t_s = 194$  days (Moriya & Tominaga 2012).  $v_s$  can be estimated from the spectral evolution.

With  $t_d$ ,  $t_s$ , and  $v_s$ , we can estimate the outer radius  $R_o$  of the CSM and the radius  $xR_o$  where the shock breakout occurs ( $R_i/R_o < x < 1$ ) for a given  $w$  based on the shock breakout model. The shock breakout condition predicts the following relations for the three values (Moriya & Tominaga 2012):

$$t_d \simeq \begin{cases} \frac{R_o}{v_s} \left[ \left( \frac{c/v_s + x^{1-w}}{c/v_s + 1} \right)^{\frac{1}{1-w}} - x \right] & (w \neq 1), \\ \frac{R_o}{v_s} \left( x^{\frac{1}{1+w}} - x \right) & (w = 1), \end{cases} \quad (5)$$

$$t_s \simeq \frac{R_o - xR_o}{v_s}. \quad (6)$$

We try three values for  $w$ :  $w = 0, 2, 5$ . The models with  $w = 2$  corresponds to the case of the steady mass loss and they are naturally expected structures for CSM. Note that X-ray observations of Type IIn SNe suggest that CSM around Type IIn SN progenitors often does not have

$w = 2$  density structures and most of the CSM is likely from non-steady mass loss (e.g., Dwarkadas & Gruszko 2011). A steep CSM density gradient with  $w = 5$  is suggested for SN 2006gy in Moriya & Tominaga (2012). We also show  $w = 0$  models which are difficult to be excluded only by the LC modeling.

It turns out in the later sections that it is difficult to estimate  $v_s$  from observational values self-consistently. This is partly because  $v_s$  is not an independent parameter and, in principle, can be derived for a given CSM structure if we specify  $E_{\text{ej}}$  and  $M_{\text{ej}}$ . However,  $v_s$  is also strongly affected by the conversion efficiency from the kinetic energy to radiation through the interaction and it is unknown at first. Thus, it is difficult to estimate  $v_s$  from the first principles. Hence, we set  $v_s$  as a free parameter in this paper. At first, we try to estimate it from the observations. As the blackbody radius of SN 2006gy expands linearly with the velocity  $5,200 \text{ km s}^{-1}$ , one may estimate that  $v_s = 5,200 \text{ km s}^{-1}$ . However, the required  $E_{\text{ej}}$  for the  $v_s = 5,200 \text{ km s}^{-1}$  models to explain the peak luminosity of SN 2006gy is found to be very high and it becomes inconsistent with the relatively low  $v_s$ . In other words, the SLSN models obtained by setting  $v_s = 5,200 \text{ km s}^{-1}$  are not self-consistent. Thus, we also try models with higher  $v_s$ , namely,  $v_s = 10,000 \text{ km s}^{-1}$ . The  $v_s = 10,000 \text{ km s}^{-1}$  models are found to work well self-consistently as is shown in the following sections. In addition, the linear evolution of the blackbody radius with  $5,200 \text{ km s}^{-1}$  is found to be able to be explained by the  $v_s = 10,000 \text{ km s}^{-1}$  models. With  $t_d = 70$  days,  $t_s = 194$  days, and the given  $v_s$ , we can derive  $R_o$  and  $xR_o$  from Equations (5) and (6) for a specified  $w$ . In the rest of this section, we show the details of the two  $v_s$  models.

#### 4.2.1 $v_s = 5,200 \text{ km s}^{-1}$ Model

This model corresponds to the SN 2006gy model in Moriya & Tominaga (2012). The shock velocity  $v_s = 5,200 \text{ km s}^{-1}$  is estimated from the observed evolution of

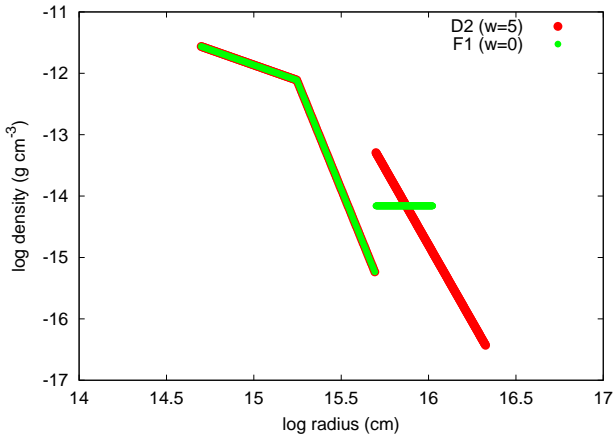


**Figure 1.** The density structures of the models D2 ( $w = 5$ ) and F1 ( $w = 0$ ) before the collision. These density structures are set as the initial conditions of the numerical LC calculations. The structure inside the density jump corresponds to the SN ejecta which is assumed to be freely expanding before the collision (Section 4.1). The dense CSM exists above the density jump. The initial condition of the dense CSM is obtained based on the shock breakout model within the CSM (Section 4.2).

the blackbody radius of SN 2006gy (Smith et al. 2010). For  $w = 5$ , we get  $R_o = 1.1 \times 10^{16}$  cm and  $xR_o = 1.8 \times 10^{15}$  cm from Equations (5) and (6). The inner radius  $R_i$  of CSM cannot be constrained by the above observables and it is a free parameter. Two  $R_i$  are tried:  $10^{15}$  cm (A1) and  $1.5 \times 10^{15}$  cm (A2). With  $w = 2$  (steady mass loss), we get  $R_o = 8.8 \times 10^{15}$  cm and  $xR_o = 9.0 \times 10^{13}$  cm (B1). We set  $R_i = xR_o$  in the  $w = 2$  models. The results do not depend so much on  $R_i$  in this case because most of the mass in the  $w = 2$  CSM is distributed in the outer part of the CSM. We also calculate LCs from the model (B2) in which the CSM mass is artificially increased 30 times of the model B1.

In  $w = 0$  models,  $t_s$  becomes similar to  $t_d$  ( $t_s \simeq t_d$ ) (Moriya & Tominaga 2012). Thus, the entire CSM is shocked with  $t_d$  and no unshocked wind remains after the LC peak. This is against the observations of SN 2006gy because narrow P-Cygni profiles are observed after the LC peak. However, this is only true when we only think a single  $w = 0$  CSM component. If there is another CSM component outside the main CSM which is not dense enough to affect the LC but the spectra, SN 2006gy-like SNe can appear. Thus,  $w = 0$  models are difficult to be excluded only by the LC. From the rising time of the LC, we can presume  $y_1 R_o - xR_o \simeq R_o - xR_o \simeq v_s t_d = 3.1 \times 10^{15}$  cm.  $y_1 R_o$  is the radius where the optical depth from the surface of the CSM becomes 1 and  $y_1 R_o \simeq R_o$  when  $w = 0$  (see Moriya & Tominaga 2012 for the details). We set the last scattering surface of the  $w = 5$  model ( $y_1 R_o = 4.9 \times 10^{15}$  cm) as  $R_o$  so that we can compare the results with those of the  $w = 5$  models. Thus,  $xR_o = 1.8 \times 10^{15}$  cm is also the same as the  $w = 5$  model and we adopt  $R_i = 10^{15}$  cm (C1).

#### 4.2.2 $v_s = 10,000$ km s $^{-1}$ Model

$v_s = 10,000$  km s $^{-1}$  models are constructed by following the same way as the  $v_s = 5,200$  km s $^{-1}$  models. With  $t_d = 70$

days,  $t_s = 194$  days, and  $v_s = 10,000$  km s $^{-1}$ ,  $R_o = 2.1 \times 10^{16}$  cm and  $xR_o = 4.6 \times 10^{15}$  cm are obtained for  $w = 5$ . We try two  $R_i$ :  $4.5 \times 10^{15}$  cm (D1) and  $5 \times 10^{15}$  cm (D2 - D7). Although  $R_i = 5 \times 10^{15}$  cm is slightly larger than the shock breakout radius  $xR_o = 4.6 \times 10^{15}$  cm, it turns out that the model gets closer to the SN 2006gy LC. Given the approximated way of our estimations, the difference is within an acceptable range. The steady mass-loss models ( $w = 2$ ) gives  $R_o = 1.7 \times 10^{16}$  cm and  $xR_o = 3.2 \times 10^{14}$  cm (E1, E2). For  $w = 0$ ,  $R_o - xR_o \simeq v_s t_d = 6 \times 10^{15}$  cm (c.f.  $y_1 R_o \simeq R_o$ ). As  $y_1 R_o = 1.1 \times 10^{16}$  cm in  $w = 5$  model, we adopted  $R_o = 1.1 \times 10^{16}$  cm and  $xR_o = R_i = 5 \times 10^{15}$  cm (F1).

## 5 LIGHT CURVE MODELS

Starting from the initial conditions obtained in Section 4, we perform the numerical LC calculations with STELLA. We show that the  $v_s = 5,200$  km s $^{-1}$  models cannot explain the huge luminosity of SN 2006gy self-consistently. LCs obtained from  $v_s = 10,000$  km s $^{-1}$  models are broadly consistent with the observational properties of SN 2006gy.

### 5.1 $v_s = 5,200$ km s $^{-1}$ Model

Figure 2 shows the LCs from the  $v_s = 5,200$  km s $^{-1}$  models with the observed  $R$  band LC of Smith et al. (2007).  $E_{ej}$  is chosen so that the peak luminosities of the model LCs can be as luminous as that of SN 2006gy. However,  $E_{ej}$  should be very high ( $\simeq 5 \times 10^{52}$  erg) for the  $v_s = 5,200$  km s $^{-1}$  models to be as luminous as SN 2006gy and assuming the relatively low  $v_s = 5,200$  km s $^{-1}$  is not consistent with the high kinetic energy. This inconsistency can also be seen from the rising times of the models. Although the models are constructed so that the rising times of the LCs become  $t_d = 70$  days, the rising times of the numerical results are much shorter than 70 days. If we set smaller  $E_{ej}$ , the rising times can be the same as that of SN 2006gy but then the luminosities become much smaller than that of SN 2006gy. Shortly, the models derived by assuming  $v_s = 5,200$  km s $^{-1}$  are not compatible with the large luminosity of SN 2006gy. Given these results, we adopt models with a higher  $v_s$ ,  $v_s = 10,000$  km s $^{-1}$ , and they are found to be able to explain the LC of SN 2006gy self-consistently (Section 5.2).

One important question of the interaction model is whether the CSM from the steady mass loss ( $w = 2$ ) can explain the properties of SLSNe and we look into the  $w = 2$  models more carefully. If it can, a mechanism to achieve such huge steady mass loss may exist. If not, it is indicated that explosive non-steady mass loss takes place in their progenitors and there should exist some mechanisms to cause such mass loss just before their explosions.

The  $w = 2$  model B1 reaches only  $\simeq -19.5$  mag in the  $R$  band at the LC peak. This is because  $M_{CSM} = 0.83M_\odot$  in the B1 model is much smaller than  $M_{CSM}$  of the models with the other  $w$ . The fraction of kinetic energy converted to radiation in the model B1 is much smaller than those in the models A1, A2, and C1, as the amount of energy converted from kinetic energy to radiation strongly depends on the relative mass of CSM and SN ejecta (see Section 6.1). Thus, more kinetic energy is required for the B1 model to be

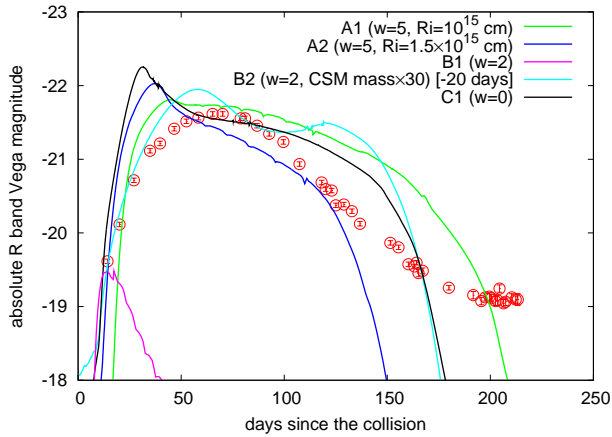


**Figure 2.** Absolute  $R$  band LCs of the  $v_s = 5,200 \text{ km s}^{-1}$  models. These models are not self-consistent. The origin of time axis is set to when our numerical calculations start, i.e., when the SN ejecta and CSM start to collide, except for B2. The time of the model B2 is shifted  $-20$  days.

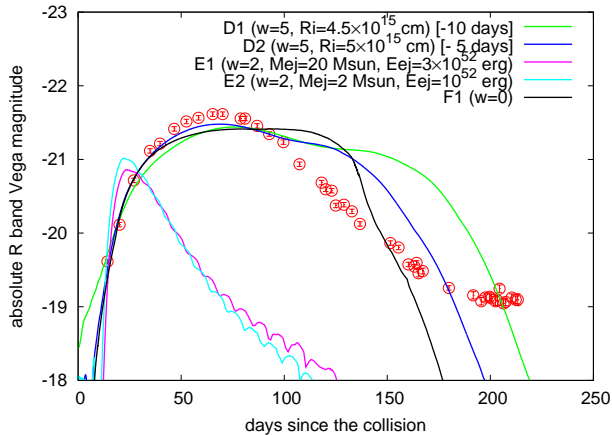


**Figure 3.** Absolute  $R$  band LCs of the  $v_s = 10,000 \text{ km s}^{-1}$  models. These models can self-consistently explain the rising time and the peak luminosity of SN 2006gy. The origin of the time axis is  $+10$  days (D1),  $+5$  days (D2),  $0$  days (E1, E2, and F1) since the collision.

as luminous as SN 2006gy. However, the rising time of the B1 model is already much less than that of SN 2006gy and it becomes shorter if we increase kinetic energy. Thus, the  $v_s = 5,200 \text{ km s}^{-1}$  model with the steady wind ( $w = 2$ , B1) is hard to be compatible with SN 2006gy. For demonstration, we also calculated a model (B2) in which  $M_{\text{CSM}}$  is increased 30 times more than that of the model B1. Then, the amount of energy converted increases because of the high efficiency for the energy conversion. In addition, the photospheric radius is increased due to the increased density. As a result, the luminosity of the model becomes as large as that of SN 2006gy.

## 5.2 $v_s = 10,000 \text{ km s}^{-1}$ Model

As  $v_s = 5,200 \text{ km s}^{-1}$  models are not able to explain SN 2006gy self-consistently, we investigate models with higher  $v_s$ ,  $v_s = 10,000 \text{ km s}^{-1}$ .  $v_s = 5,200 \text{ km s}^{-1}$  is estimated from the evolution of the blackbody radius but it is shown that the evolution of the blackbody radius in the  $v_s = 10,000 \text{ km s}^{-1}$  models is consistent with that of SN 2006gy.

### 5.2.1 Light Curve

The  $R$  band LCs from the  $v_s = 10,000 \text{ km s}^{-1}$  models are shown in Figure 3. Multicolor LCs of the models D2 ( $w = 5$ ) and F1 ( $w = 0$ ) are shown in Figure 4 and the bolometric LCs of the two models are shown in Figure 5. The color evolution of the models D2 and F1 are shown in Figure 6.

The rising parts and the peak luminosities of the LCs of the  $w = 0, 5$  models are consistent with SN 2006gy. Thus, the  $v_s = 10,000 \text{ km s}^{-1}$  models are self-consistent with the assumed  $E_{\text{ej}}$  and  $M_{\text{ej}}$ . The  $v_s = 10,000 \text{ km s}^{-1}$  models only require  $E_{\text{ej}} = 10^{52}$  erg to achieve the peak luminosity of SN 2006gy, instead of  $E_{\text{ej}} \simeq 5 \times 10^{52}$  erg required for the  $v_s = 5,200 \text{ km s}^{-1}$  models. This is because the blackbody radius in the CSM can be larger in the  $v_s = 10,000 \text{ km s}^{-1}$  models and less energy is required to achieve the same luminosity. The steady mass-loss models ( $w = 2$ ) are, however, still not consistent with SN 2006gy.

The model LCs with  $w = 0, 5$  after the peak start to deviate from the observed LCs, although the deviations stay less than one magnitude before the plateau in the observed LC at around 200 days. Our model  $R$  band LCs take some time after the LCs have reached the peak until the LCs start to decline, contrary to the observed  $R$  band LC of SN 2006gy. This is because there remains unshocked optically thick CSM even after the LC peak in our numerical models and the photosphere remains there for a while. The analytic model of Moriya & Tominaga (2012) which we use for the estimate of the initial condition assumes a constant  $v_s$ . However,  $v_s$  actually reduces as the interaction goes on and the optically thick part of CSM does not shocked away entirely at the time  $t_d$  when the optically thick CSM is assumed to be swept up by the forward shock in the model of Moriya & Tominaga (2012). This effect is more significant in  $w = 0$  models because  $w = 0$  models suffer more on the deceleration than  $w = 5$  models. A severe failure of our models is that all of them fail to reproduce the plateau in the LC of SN 2006gy at around 200 days. We discuss this separately in Section 6.2.

Looking at the multicolor LCs (Figure 4), the  $w = 0$  model (F1) is closer to the observed LC, especially the  $B$  band LC of the rising epochs. This is presumed to be because the initial density jump between SN ejecta and CSM is smaller in the  $w = 0$  model (Figure 1) and the temperature becomes lower in the  $w = 0$  model. However, the LCs in the  $U$  and  $B$  bands can be affected by many weak absorption lines of Fe group elements which are not taken into account in our opacity. Those weak absorptions may reduce the luminosity of the  $U$  and  $B$  band LCs and we cannot judge which model is better based just on the blue part of the LCs. In addition, the difference is  $\simeq 0.5$  mag and they are not significant. The color evolution of the two models



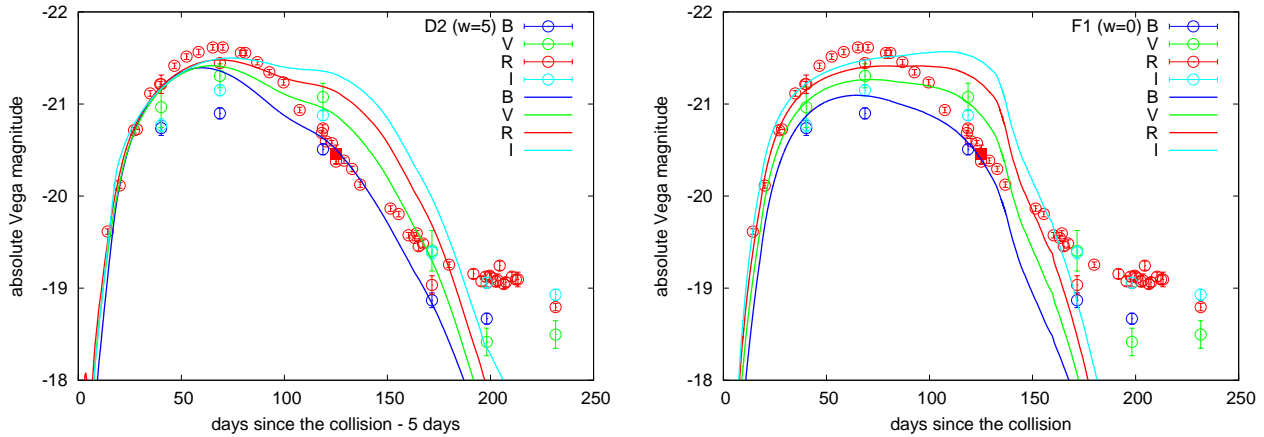


**Figure 4.** Multicolor LCs of the models D2 ( $w = 5$ , left) and F1 ( $w = 0$ , right). The observational data are from Smith et al. (2007); Agnoletto et al. (2009); Kawabata et al. (2009). The origin of the time axis in the left (right) panel is 5 (0) days since the collision.

(Figure 6) roughly follows the observed evolution, although there exist some deviations especially in  $R - I$  and  $V - R$ .

Although it is possible to continue LC modeling to get much better fits to the SN 2006gy LC, it does not necessarily lead us to the better understanding of the properties of the SN ejecta and the dense CSM involved in the progenitor system of SN 2006gy. This is mainly because of the simplified physics adopted in STELLA. Especially, STELLA is a one-dimensional code and multidimensional effects are approximately incorporated by adopting the smearing parameter. As the uncertainties involved in the parameter are large (see Section 5.2.4), making a perfect fit to the observed LC does not necessarily provide us with the best parameter. In addition, the differences in the LCs in the declining phases are less than one magnitude (or a factor  $\simeq 2$ ) and the differences in the rising phases are much less. Thus, the properties of the SN ejecta and the dense CSM in the D2 and F1 models are presumed not to be so different from the 'actual' values. Thus, we conclude that the CSM parameters predicted by the shock breakout model can explain the overall properties of SN 2006gy. We also note that a systematical study of the effect of the CSM properties on the LCs powered by the interaction between SN ejecta and dense CSM is summarized in Moriya et al. (2011). The durations of the LCs of the models D2 and F1 are a bit longer than that of SN 2006gy. To reduce the durations of the LCs by keeping the peak luminosities of them, we can, for example, change the radii of the CSM.

Finally, we look into the steady mass loss models to see whether they actually fail to reproduce the LC of SN 2006gy. The steady mass-loss model ( $w = 2$ , E1) is, again, too faint to explain SN 2006gy with  $E_{\text{ej}} = 3 \times 10^{52}$  erg. The rising time is already too short and reaching the peak luminosity of SN 2006gy by increasing  $E_{\text{ej}}$  does not work as is discussed in Section 5.1. This is because of the too small  $M_{\text{CSM}}$  and can be improved if  $M_{\text{CSM}}$  is increased (see the models B1 and B2). Another possible way to make  $w = 2$  models work is to increase the conversion efficiency from  $E_{\text{ej}}$  to radiation energy so that  $E_{\text{ej}}$  can be reduced (see Section 6.1 for the discussion of the conversion efficiency). In the model E2,  $M_{\text{ej}}$  is set to be comparable to  $M_{\text{CSM}}$  so that

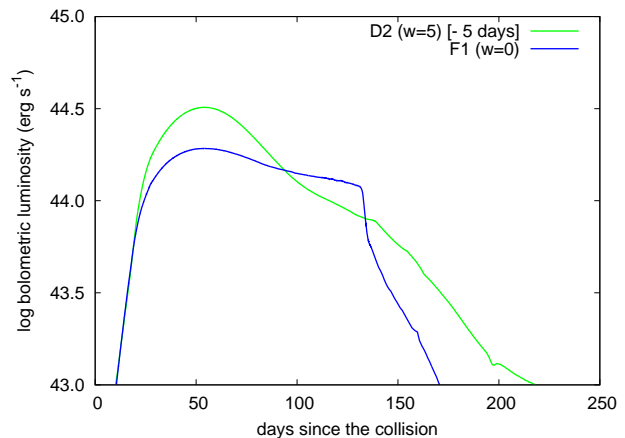


**Figure 5.** Bolometric LCs of the models D2 ( $w = 5$ ) and F1 ( $w = 0$ ). The origin of the time axis in the D2 (F1) model is 5 (0) days since the collision.

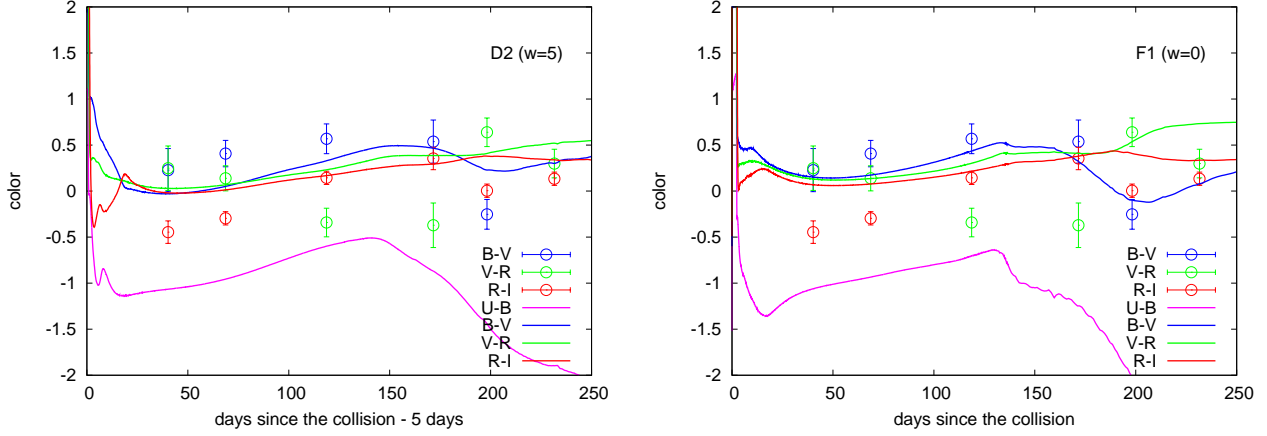
the conversion efficiency becomes higher (Section 6.1). The similar peak luminosity to the model E1 is reached with less  $E_{\text{ej}}$  ( $10^{52}$  erg) in the model E2. However, as the diffusion time of the CSM is not affected so much by this, the LCs become similar to each other and increasing the efficiency does not revive the  $w = 2$  models. To summarize, the dense CSM from the steady mass loss is still difficult to explain the LC of SN 2006gy with the shock breakout model.

### 5.2.2 Dynamical Evolution

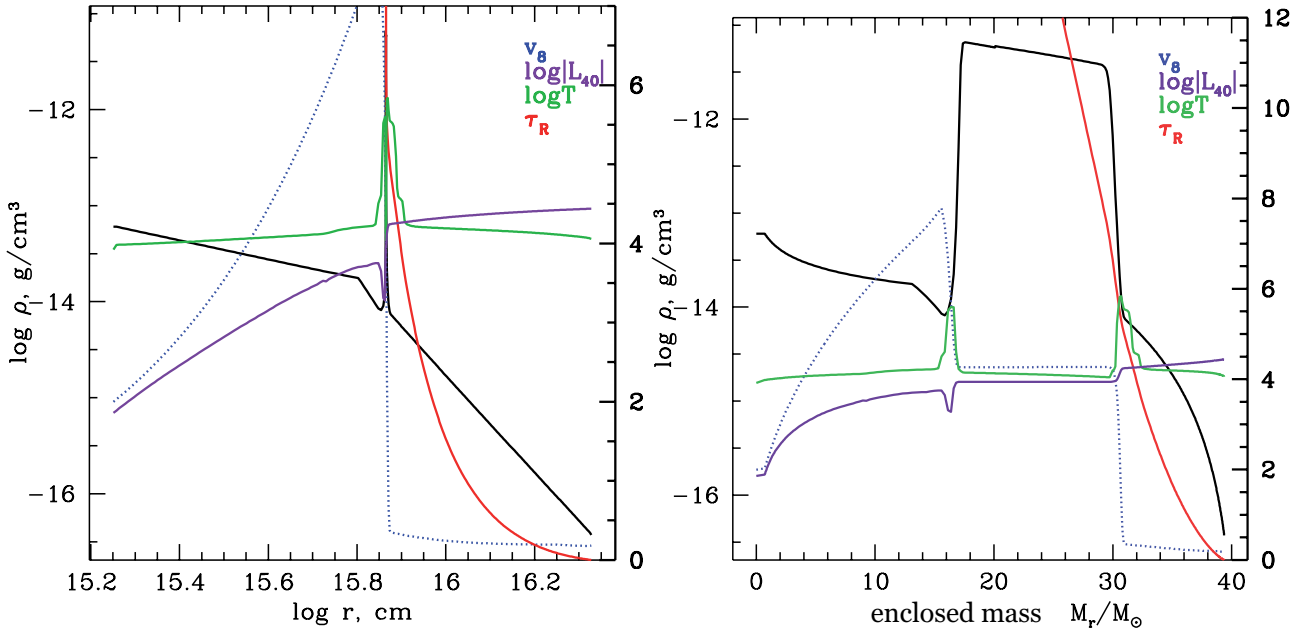
Figure 7 shows the dynamical structures of the model D2 ( $w = 5$ ) at around the LC peak. The left panel shows the structure in the physical coordinate (radius) whereas the right panel shows the structure in the mass coordinate. The cool dense shell is created between SN ejecta and CSM in which about  $10 M_{\odot}$  of shocked CSM and  $3 M_{\odot}$  of shocked SN ejecta are contained.

Figure 8 shows the evolution of the color temperature ( $T_{\text{col}}$ ) and the effective temperature ( $T_{\text{eff}}$ ) of the model





**Figure 6.** Color evolution of the models D2 ( $w = 5$ , left) and F1 ( $w = 0$ , right). Observational points are from Agnoletto et al. (2009).



**Figure 7.** Physical structures of the model D2 in radius (left) and mass coordinate (right) at around the LC peak (74 days since the collision). Black lines show the density structure (left  $y$ -axis). Blue dotted lines are the velocity scaled by  $10^8 \text{ cm s}^{-1}$  (right  $y$ -axis), purple lines are the logarithm of the absolute value of luminosity scaled by  $10^{40} \text{ erg s}^{-1}$  (right  $y$ -axis), green lines are the logarithm of the temperature in Kelvin (right  $y$ -axis), and red lines are Rosseland optical depth measured from the outside (right  $y$ -axis).

D2. The color temperature is derived by fitting the spectra obtained by the numerical calculations with the blackbody spectral distribution whereas the effective temperature is obtained by using the bolometric luminosity ( $L_{\text{bol}}$ ) and the radius ( $R_{\tau_R=2/3}$ ) of the photosphere which is defined as the radius where the Rosseland mean optical depth  $\tau_R$  from the surface becomes  $2/3$  in STELLA and is expressed as  $T_{\text{eff}} = (L_{\text{bol}}/4\pi\sigma R_{\tau_R=2/3}^2)^{1/4}$ . Here,  $\sigma$  is the Stephan-Boltzmann constant. As radiation mainly comes from the shell and the Thomson scattering is the dominant opacity source in the CSM above the shell,  $T_{\text{col}}$  roughly traces the temperature of the shell. The photosphere ( $R_{\tau_R=2/3}$ ) is much above the shell and  $T_{\text{eff}}$  becomes very low because of the large  $R_{\tau_R=2/3}$  (see also Figure 9). At the time when  $T_{\text{col}}$

starts to increase for the second time (from  $\simeq 180$  days), the photosphere is in the SN ejecta whose density structure and composition are expressed in the approximated way and the results around these epochs and later should not be taken seriously.

Figure 9 shows the evolution of the blackbody radius  $R_{\text{BB}} = \sqrt{L_{\text{bol}}/4\pi\sigma T_{\text{col}}^4}$  and the photosphere  $R_{\tau_R=2/3}$ . The constant velocity line with  $5,200 \text{ km s}^{-1}$  is the evolution of the blackbody radius obtained by Smith et al. (2010) along which  $R_{\text{BB}}$  follows until around 125 days. The evolution of  $R_{\text{BB}}$  in the models D2 and F1 is consistent with  $5,200 \text{ km s}^{-1}$  although the radius is a bit smaller than the observed values. The bolometric correction of Smith et al. (2010) is based on  $T_{\text{BB}}$  and the correction may add extra

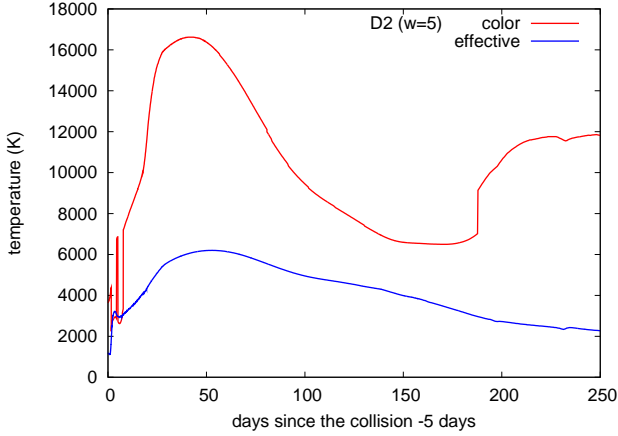


**Figure 8.** Evolution of the color temperature ( $T_{\text{col}}$ ) and the effective temperature ( $T_{\text{eff}}$ ) in the model D2. The origin of the time axis is 5 days since the collision.

luminosities because it ignores the effect of line depletion. Higher  $L_{\text{bol}}$  results in higher  $R_{\text{BB}}$  for a given  $T_{\text{col}}$  and this can be the reason why  $R_{\text{BB}}$  of Smith et al. (2010) is higher than ours.

$R_{\text{BB}}$  obtained by our calculations tends to be smaller than the shell radius where the radiation is coming from. For example,  $R_{\text{BB}}$  of the model D2 shown in Figure 9 stays lower than the radius at which the interaction starts ( $R_i = 5 \times 10^{15}$  cm). The reason is presumed to be similar to that of the discrepancy in  $R_{\text{BB}}$  obtained from observations and numerical calculations.  $T_{\text{col}}$  is obtained from the spectral fitting but actual spectra suffer from the line depletion especially in blue. Since  $T_{\text{col}}$  is reduced from the temperature at the photon production site,  $L_{\text{bol}}$  is the value affected by such depletion and is less than the value expected from the blackbody with  $T_{\text{col}}$ . Thus, with the smaller  $L_{\text{bol}}$ ,  $R_{\text{BB}} = \sqrt{L_{\text{bol}}/4\pi\sigma T_{\text{col}}^4}$  becomes smaller than the actual emitting region.

As most of hydrogen in CSM remains to be ionized,  $R_{\tau_R=2/3}$  continues to be at the radius where the Rosseland mean opacity from the surface of the CSM is 2/3 and remains to be constant until the shock wave comes close to the radius. Then,  $R_{\tau_R=2/3}$  evolves roughly following the forward shock.

### 5.2.3 $M_{\text{ej}}$ and $E_{\text{ej}}$

The properties of SN ejecta ( $M_{\text{ej}}$  and  $E_{\text{ej}}$ ) determine many aspects of SNe powered by the shock interaction (e.g., luminosities) because  $E_{\text{ej}}$  determines the available energy and  $M_{\text{ej}}$  affects the efficiency to convert the available kinetic energy to the radiation energy. We discuss the effect of  $M_{\text{ej}}$  and  $E_{\text{ej}}$  in Section 6.1 including the results of the  $v_s = 5,200$  km s $^{-1}$  models and here we just show the results of LC calculations with different  $M_{\text{ej}}$  and  $E_{\text{ej}}$  (Figure 10). LCs are similar to each others and we can see that it is difficult to constrain  $M_{\text{ej}}$  and  $E_{\text{ej}}$  only by the LC. This can also be seen by comparing the models E1 and E2 in Figure 3. The two models have different  $M_{\text{ej}}$  and  $E_{\text{ej}}$  with the same CSM but the resulting LCs are similar (see discussion in Section 6.1).

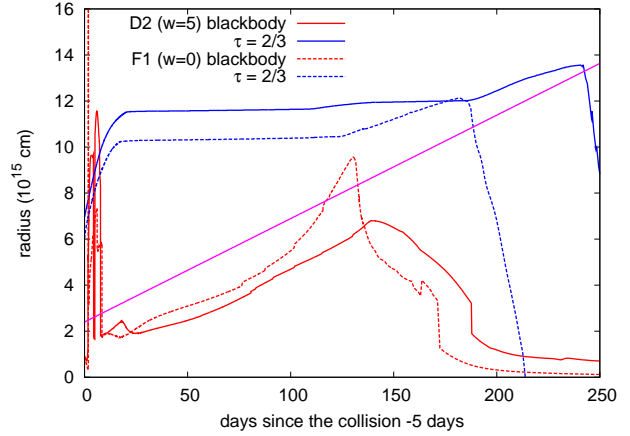


**Figure 9.** Evolution of the blackbody radius ( $R_{\text{BB}}$ , solid line) and the photospheric radius ( $R_{\tau=2/3}$ , dashed line) of the models D2 ( $w = 5$ ) and F1 ( $w = 0$ ). The origin of the time axis is 5 days since the collision. The monotonically increasing linear line at the middle is the evolution of the blackbody radius obtained by Smith et al. (2010), a constant velocity evolution with 5,200 km s $^{-1}$ . The observational blackbody radius follows the line until around 125 days and starts to decline (see Smith et al. (2010) for details).

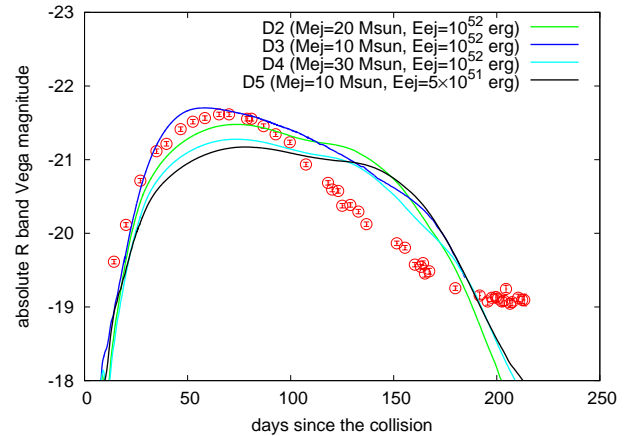


**Figure 10.**  $R$  band LCs from the same CSM but different  $M_{\text{ej}}$  and  $E_{\text{ej}}$ . The models D2, D3, D4 have the same  $E_{\text{ej}}$  but different  $M_{\text{ej}}$ , i.e.,  $10 M_{\odot}$  (D3),  $20 M_{\odot}$  (D2), and  $30 M_{\odot}$  (D3). The model D5 has less  $E_{\text{ej}}$  ( $5 \times 10^{51}$  erg) than other models ( $10^{52}$  erg) and  $M_{\text{ej}} = 10 M_{\odot}$ . The calculation of the LC of the model D3 stopped at around 175 days since the collision and we show the LC until around 175 days.

In the best LC model of the pulsational pair-instability model presented by Woosley, Blinnikov, & Heger (2007), the ejecta with  $5.1 M_{\odot}$  and  $2.9 \times 10^{51}$  erg collides the CSM with  $24.5 M_{\odot}$ . Our canonical models (D2 and F1) have much higher  $E_{\text{ej}}$  ( $10^{52}$  erg). One of the reasons is presumed to be the smaller photospheric radius ( $y_1 R_o = 1.1 \times 10^{16}$  cm) in our models. The dense CSM in the pulsational pair-instability model extends to about  $3 \times 10^{16}$  cm and the photosphere can be larger than our models. This effect of the locations of the photosphere can also be seen in comparison to the  $v_s = 5,200$  km s $^{-1}$  models. The photospheric radii of

them are only  $y_1 R_o \simeq 5 \times 10^{15}$  cm at most and the required energy to achieve the maximum luminosity of SN 2006gy is  $5 \times 10^{52}$  erg which is even larger than  $10^{52}$  erg required for the  $v_s = 10,000$  km s $^{-1}$  models ( $y_1 R_o = 1.1 \times 10^{16}$  cm). This shows the difficulties to constrain  $E_{ej}$  only by the LC.

In addition, the efficiency to convert the kinetic energy to radiation is mainly determined by the relative mass of the ejecta and the collided CSM. It does not depend strongly on the ejecta mass if the CSM mass is much larger than the ejecta mass. To get high conversion efficiencies of the kinetic energy to the radiation energy,  $M_{ej}$  is better to be comparable or less than  $M_{CSM}$  and we can at least get some constraint on  $M_{ej}$  from the LC based on the view point of the conversion efficiency (Section 6.3).

#### 5.2.4 Smearing

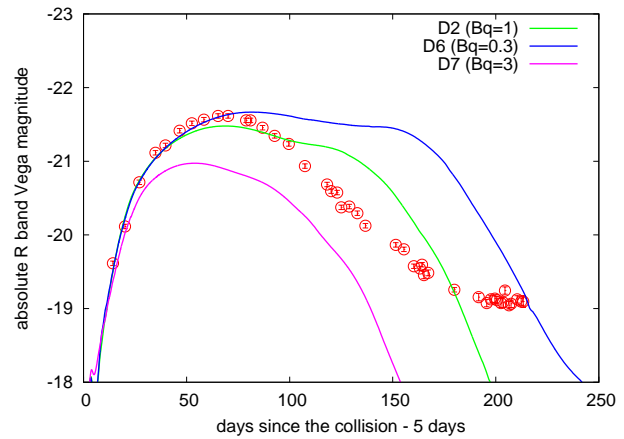
The dense shell which appears between SN ejecta and CSM is unstable in multidimension as is discussed in Section 3.2. As a result of the instabilities, less kinetic energy is expected to be converted to radiation because there would be the extra multidimensional motions caused by the instabilities. To take into account such multidimensional effects in one-dimensional code STELLA, we include a smearing term in the equation of motion (the parameter  $B_q$ , Section 3.2).

Figure 11 shows the LCs with different values of the smearing parameter  $B_q$ . With larger  $B_q$ , the effect of the smearing becomes larger and less kinetic energy is converted to radiation. In other words, radiative cooling becomes less efficient. The model D2 is calculated with our standard  $B_q = 1$ . The model D6 has  $B_q = 0.33$  and the model D7 has  $B_q = 3$ . The shape of the LC is different even if we only change  $B_q$  with a factor 3. We also show the effect of  $B_q$  on the LCs obtained from the pulsational pair-instability SN models of Woosley, Blinnikov, & Heger (2007) in Appendix A and show that the effect is not unique to our models. We discuss the efficiency in detail in Section 6.1.

The uncertainty in the smearing parameter adds another difficulty in our estimations of physical parameters of the progenitor system. This is one reason why we think that making the perfect fitting now does not lead us to the exact parameters of the progenitor system. The calibrations for the smearing parameter should be done at least. However, the rising time and the peak luminosity is not so sensitive to the smearing parameter and the parameters of SN ejecta and dense CSM we obtain with the current uncertainty are presumed to be close to the real ones.

#### 5.2.5 Effect of $^{56}\text{Ni}$

We have also examined the effect of  $^{56}\text{Ni}$  decay on the LCs. Figure 12 shows the results. We include  $^{56}\text{Ni}$  at the center of the model D2. If we include  $^{56}\text{Ni}$ , the length of the peak is extended due to the extra heat source. The significant effect can only be seen when we include  $\sim 10 M_\odot$  of  $^{56}\text{Ni}$ . However, the amount of  $^{56}\text{Ni}$  is observationally constrained to be less than  $2.5 M_\odot$  (Miller et al. 2010) and the effect of  $^{56}\text{Ni}$  is negligible.



**Figure 11.** R band LCs with different  $B_q$ , i.e., D2 ( $B_q = 1$ ), D6 ( $B_q = 0.3$ ), and D7 ( $B_q = 3$ ). The smearing parameter  $B_q$  changes the conversion efficiency from kinetic energy to radiation. With Larger  $B_q$ , more kinetic energy remains and less radiation energy is emitted. The origin of the time axis is 5 days since the collision.

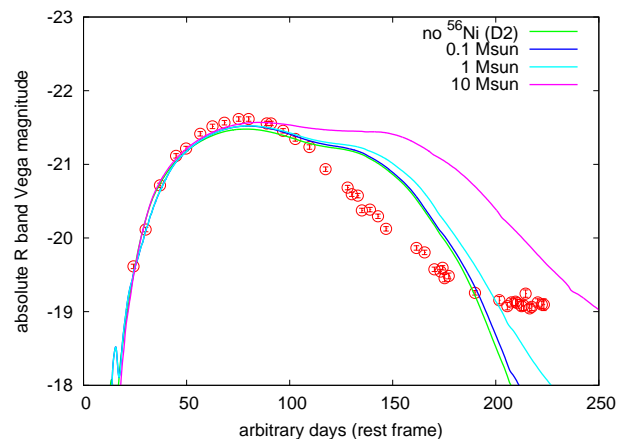


**Figure 12.** R band LCs with  $^{56}\text{Ni}$ . 0.1  $M_\odot$ , 1  $M_\odot$ , and 10  $M_\odot$  of  $^{56}\text{Ni}$  is included at the center of the model D2. Only 10  $M_\odot$  of  $^{56}\text{Ni}$  makes significant effect on the LC.

## 6 DISCUSSION

### 6.1 Conversion Efficiency

The source of radiation in our LC models is the kinetic energy of SN ejecta. The amount of energy converted from kinetic energy to radiation can be estimated by the conservation laws of energy and momentum. If we assume that the radiation pressure does not change the dynamics of the materials so much, the conservation of momentum requires

$$M_{\text{colej}} v_{\text{colej}} = (M_{\text{colej}} + M_{\text{sCSM}}) v_{\text{shell}}, \quad (7)$$

where  $M_{\text{colej}}$  is the mass of the collided SN ejecta,  $v_{\text{colej}}$  is the mean velocity of the collided SN ejecta,  $M_{\text{sCSM}}$  is the mass of the shocked CSM, and  $v_{\text{shell}}$  is the velocity of the dense shell between SN ejecta and CSM. Radiation energy  $E_{\text{rad}}$  emitted as a result of the interaction can be derived

from the conservation of energy

$$E_{\text{rad}} = \alpha \left[ \frac{1}{2} M_{\text{colej}} v_{\text{colej}}^2 - \frac{1}{2} (M_{\text{colej}} + M_{\text{sCSM}}) v_{\text{shell}}^2 \right], \quad (8)$$

where  $\alpha$  is the fraction of kinetic energy converted to radiation. From Equations (7) and (8),

$$\frac{E_{\text{rad}}}{\frac{1}{2} M_{\text{colej}} v_{\text{colej}}^2} = \frac{\alpha M_{\text{sCSM}}}{M_{\text{colej}} + M_{\text{sCSM}}}. \quad (9)$$

If most of the SN ejecta and CSM are shocked, i.e.,  $M_{\text{colej}} \simeq M_{\text{ej}}$  and  $M_{\text{sCSM}} \simeq M_{\text{CSM}}$ , we get the rough estimate for the radiation energy emitted

$$E_{\text{rad}} \simeq \frac{\alpha M_{\text{CSM}}}{M_{\text{ej}} + M_{\text{CSM}}} E_{\text{ej}}. \quad (10)$$

$\alpha$  is expected to be close to 1 without the smearing parameter  $B_q$  because most of thermal energy gained by the shock is eventually emitted as radiation. Since the parameter  $B_q$  adds additional acceleration to reduce the amount of energy converted to thermal energy,  $\alpha$  is expected to become lower as  $B_q$  becomes larger. The rest of energy is mostly in the form of kinetic energy. We may also express the effect as the reduction of the radiative cooling efficiency because less radiation energy is emitted with the smearing term.

Table 2 is the list of radiation energy which is obtained by adding up the bolometric luminosity from the time of collision to around 300 days since the collision. The model D3 is excluded because we do not have the entire numerical LC. We also show the parameter  $\alpha$  which is derived by using Equation (10). The efficiency  $E_{\text{rad}}/E_{\text{ej}}$  to convert SN kinetic energy to radiation is plotted in Figure 13 as a function of  $M_{\text{CSM}}/(M_{\text{ej}} + M_{\text{CSM}})$  with the results obtained by van Marle et al. (2010).

At the high  $M_{\text{CSM}}/(M_{\text{ej}} + M_{\text{CSM}})$  region, our standard  $B_q = 1$  results follow the line of  $\alpha = 0.5$ . This means that the efficiency to convert the kinetic energy to radiation is reduced by 50%. On the other hand, the results of van Marle et al. (2010) follow the  $\alpha = 1$  line and the effect of multidimensional instabilities is not significant. Although van Marle et al. (2010) use a three-dimensional code and multidimensional instabilities are included in principle, their approximated way to treat the radiation and limited spatial resolution may have prevented multidimensional instabilities from growing.

As  $M_{\text{CSM}}/(M_{\text{ej}} + M_{\text{CSM}})$  becomes lower, the results start to deviate from the constant  $\alpha$  line. This is because  $M_{\text{CSM}}$  gets very small and most of the ejecta is not affected by the interaction, i.e., the assumption  $M_{\text{colej}} = M_{\text{ej}}$  is no longer valid and Equation (10) should not be used. We should use Equation (8) instead. As  $M_{\text{colej}} \ll M_{\text{ej}}$  in this regime, the efficiencies tend to be higher than the values obtained from Equation (10).

The combinations of  $E_{\text{ej}}$  and  $M_{\text{ej}}$  which give a similar  $[M_{\text{sCSM}}/(M_{\text{colej}} + M_{\text{sCSM}})] \frac{1}{2} M_{\text{colej}} v_{\text{ej}}^2$  are expected to result in similar LCs and they are degenerated. Thus, it is difficult to constrain the exact value for  $M_{\text{ej}}$  and  $E_{\text{ej}}$  from LCs. This is clearly seen in the models E1 and E2 in Figure 3. Both the models have similar LCs. The CSM of the two models is exactly the same but  $M_{\text{ej}}$  and  $E_{\text{ej}}$  are different. Although  $M_{\text{colej}} < M_{\text{ej}}$  in the model E1 and  $M_{\text{colej}} \simeq M_{\text{ej}}$  in the model E2,  $M_{\text{colej}}$  and  $\frac{1}{2} M_{\text{colej}} v_{\text{ej}}^2$  are happened to be similar in the two models with the similar  $M_{\text{sCSM}} \simeq M_{\text{CSM}}$ . Thus, the two

**Table 2.** Conversion Efficiency from Kinetic Energy to Radiation Energy

Name	$E_{\text{rad}}$ $10^{51}$ erg	$E_{\text{rad}}/E_{\text{ej}}$	$\frac{M_{\text{CSM}}}{M_{\text{ej}} + M_{\text{CSM}}}$	$\alpha$
A1	13	0.25	0.52	0.48
A2	12	0.24	0.33	0.72
B1	0.46	0.046	0.040	1.1
B2	8.7	0.29	0.57	0.50
C1	14	0.28	0.41	0.68
D1	2.7	0.27	0.52	0.51
D2	2.2	0.22	0.47	0.47
E1	2.6	0.086	0.14	0.63
E2	3.0	0.30	0.62	0.48
F1	2.9	0.29	0.64	0.46
D4	1.7	0.17	0.38	0.46
D5	1.6	0.32	0.64	0.50
D6	3.4	0.34	0.47	0.72
D7	0.89	0.089	0.47	0.19

models have similar  $[M_{\text{sCSM}}/(M_{\text{colej}} + M_{\text{sCSM}})] \frac{1}{2} M_{\text{colej}} v_{\text{ej}}^2$  and result in the similar LCs.

## 6.2 Origin of the Plateau Phase

There exists a plateau in the LC of SN 2006gy at around 200 days. None of our models is succeeded in producing the plateau. This is because the remaining CSM at these epochs is too thin to affect the LC. Note that the LC observations at later epochs reject the possibility to explain this plateau by  $^{56}\text{Ni}$  heating (see also Section 5.2.5). There are several other possible ways to explain the plateau. One possibility is the recombination in the SN ejecta. Because we use the simplified SN ejecta structures, our results of LC calculations after the photosphere gets inside of the SN ejecta are beyond the applicability of our simple models. Increasing the SN ejecta mass may also help because a plateau phase can be longer with larger hydrogen mass, although the conversion efficiency from kinetic energy to radiation is also affected at the same time (Section 6.1). By putting more realistic SN ejecta with realistic hydrogen-rich envelopes or more massive SN ejecta, the recombination wave may stay the envelope for a while and may end up with the plateau phase, as is the case in Type IIP SNe (see, e.g., Kasen & Woosley 2009). We note that the blackbody temperatures of these epochs are  $\simeq 6000$  K and they are consistent with this scenario. Recombination may also occur in the shocked CSM or dense cool shell.

Light echoes from the remaining CSM may also play a role. The LC after this plateau phase remains almost constant for more than 200 days, although the luminosity is about 10 times smaller (Miller et al. 2010). Thus, it is possible that there existed another CSM component which caused the echoes at around 200 days and shocked away when SN 2006gy was behind the Sun.

Smearing may also be relevant to the plateau. In the models in Appendix A, we can see that the plateau can appear or disappear depending on the degree of the smearing. Less smearing makes the cool shell denser and photosphere can stay there for a longer time, possibly making the plateau phase.

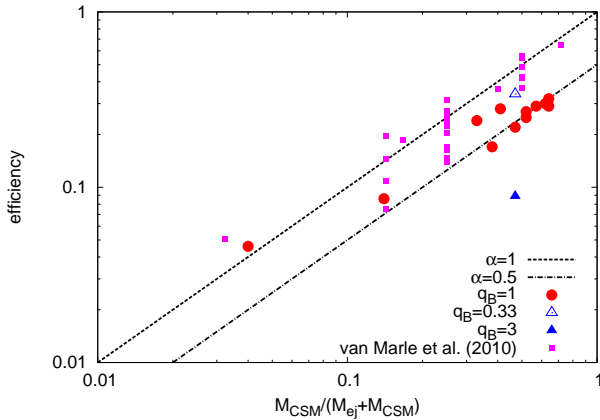


**Figure 13.** Efficiency of the conversion of kinetic energy to radiation. Most of the results from van Marle et al. (2010), including aspherical models, are also shown.  $\alpha$  is the measure for the effect of the smearing parameter  $B_q$ .  $\alpha = 1$  means NO smearing effect and the smearing effect increases as  $\alpha$  gets small.

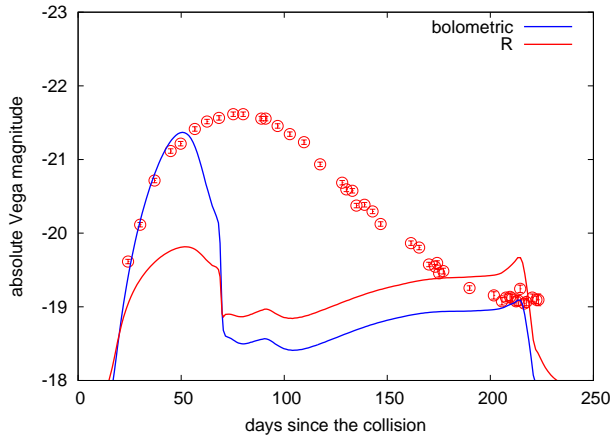


**Figure 14.** Observed  $R$  band LC and the bolometric and  $R$  band LCs calculated with the parameter shown in Chatzopoulos, Wheeler, & Vinko (2012). The observational points are shifted arbitrarily to match the numerical result in the figure.

### 6.3 Progenitor of SN 2006gy

As the properties of the progenitor system which can be obtained from the LC modeling strongly depends on CSM, it is difficult to get information on the progenitor from the LC of SN 2006gy. The CSM properties and SN ejecta properties are degenerated. However, we can get some indications for it. As the origin of the luminosity is the kinetic energy of SN ejecta, the kinetic energy should be converted to radiation efficiently. If  $M_{\text{CSM}} \ll M_{\text{ej}}$ , the conversion efficiency  $\alpha M_{\text{CSM}} / (M_{\text{ej}} + M_{\text{CSM}})$  is so small that the kinetic energy cannot be converted efficiently enough to explain the LC of SN 2006gy. Thus, the mass of the CSM should be close to or larger than  $M_{\text{ej}}$ .

According to our modeling,  $M_{\text{CSM}}$  is required to be  $\sim 10 M_{\odot}$  and this means that  $M_{\text{ej}}$  is expected to be  $\sim 10 M_{\odot}$  or less. This indicates that the total mass of

the system well exceeds  $10 M_{\odot}$  and the progenitor of SN 2006gy should be a very massive star. In addition, the progenitor should lose  $M_{\text{CSM}}$  within  $\sim 10$  years before the explosion. Our models for SN 2006gy have  $M_{\text{CSM}} \simeq 18 M_{\odot}$  and it may be difficult for red supergiants (RSGs) to have such mass loss because of the following reason: To have CSM with  $18 M_{\odot}$ , the zero-age main-sequence mass of RSGs should be very large but such massive stars suffer more from the radiation driven wind during their main-sequence phase because of their large luminosities. Thus, losing most of their mass only just before their explosions might be difficult. However, extensive mass loss of RSGs is suggested by many authors (e.g., van Loon et al. 2005; Vanbeveren, Van Bever, & Belkus 2007; Smith, Hinkle, & Ryde 2009; Boyer et al. 2010; Yoon & Cantiello 2010; Moriya et al. 2011; Georgy 2012) and it is still possible that very massive RSGs lose  $\sim 10 M_{\odot}$  just before their explosions due to, e.g., pulsations (e.g., Yoon & Cantiello 2010; Heger et al. 1997; Li & Gong 1994), dust (e.g., van Loon et al. 2005), or g-mode oscillations (Quataert & Shiode 2012, see also Arnett & Meakin 2011).

Another possible progenitor of SN 2006gy is a very massive star in the luminous blue variable (LBV, see, e.g., Humphreys & Davidson 1994) phase which is suggested to be the progenitor of SN 2006gy (e.g., Smith et al. 2007). LBVs experience extensive mass loss and some of them, e.g.,  $\eta$  Carinae, have  $\sim 10 M_{\odot}$  CSM (e.g., Smith & Owocki 2006). Their typical wind velocities are also consistent with the wind velocities estimated from the narrow P-Cygni  $\text{H}\alpha$  profiles in SN 2006gy (e.g., Smith et al. 2010). Although LBVs are theoretically considered to be on the way to Wolf-Rayet stars and do not explode (e.g., Crowther 2007; Vink 2009), the progenitor of Type IIn SN 2005gl is found to be an LBV (Gal-Yam et al. 2007; Gal-Yam & Leonard 2009). Several other Type IIn SNe are also suggested to have evidences for LBV progenitors (e.g., Kotak & Vink 2006; Trundle et al. 2008; Smith et al. 2011; Kiewe et al. 2012).

A shell created due to the interaction between the RSG wind and the Wolf-Rayet wind is another possible way to have a massive CSM (e.g., Dwarkadas 2011). Alternatively, a shell created by pulsational instability can be followed up by the SN ejecta, instead of the ejecta of the next pulse as suggested by Woosley, Blinnikov, & Heger (2007). Some binary interaction may cause extensive mass loss (e.g., Hachisu, Kato, & Nomoto 2008) but binary systems have not been considered deeply as a possible progenitor of SLSNe yet (see Chevalier 2012; Soker 2012). The collision of massive stars in a dense stellar cluster can make a massive star surrounded by a massive CSM and it may also result in SN 2006gy-like SLSNe (Portegies Zwart & van den Heuvel 2007, see also Pan, Loeb, & Kasen 2012).

With the condition that  $M_{\text{ej}}$  is similar to or less than  $M_{\text{CSM}}$ , the conversion efficiency of kinetic energy to radiation (Equation (9)) is expected to be  $\simeq 50\%$  at most (Section 6.1). As the radiation energy emitted by SN 2006gy exceeds  $2 \times 10^{51}$  erg, the SN ejecta should have more than  $\simeq 4 \times 10^{51}$  erg. Thus, the SN explosion inside should be very energetic. As the energy of our models is comparable to those of energetic broad-line Type Ic SNe whose progenitors are suggested to be very massive (e.g., Nomoto et al. 2011), the estimated high energy may also indicate that the progenitor mass is rather close to those of LBVs. Note,

however, that the host galaxy of SN 2006gy is not metal-poor (e.g., Ofek et al. 2007) while broad-line Type Ic SNe appear more preferentially in low metallicity environments (e.g., Arcavi et al. 2010; Modjaz et al. 2011; Sanders et al. 2012). In addition, the late time spectra of SN 2006gy are not similar to those of broad-line Type Ic SNe (Kawabata et al. 2009), although the late time spectra of Type Ic SLSN 2010gx show such features (Pastorello et al. 2010).

#### 6.4 Comparison to Semi-Analytic Model

Recently, Chatzopoulos, Wheeler, & Vinko (2012) proposed a semi-analytic model of LCs powered by the shock interaction. The model involves several simplifications but the overall features predicted by the model are shown to match some numerical results. They show a LC model of SN 2006gy and we perform LC calculations with the same parameters which are obtained by them. The parameters are  $\delta = 0$ ,  $n = 12$ ,  $w = 0$ ,  $E_{ej} = 4.4 \times 10^{51}$  erg,  $M_{ej} = 40 M_{\odot}$ ,  $R_i = 5 \times 10^{14}$  cm, and  $R_o = 2.5 \times 10^{15}$  cm (corresponds to  $M_{CSM} = 5 M_{\odot}$  with a constant CSM density  $1.5 \times 10^{-13}$  g cm $^{-3}$ ). Following the result of Chatzopoulos, Wheeler, & Vinko (2012), we put  $2 M_{\odot}$  of  $^{56}\text{Ni}$  at the center of the ejecta but the value is too small to affect the main part of the LC (Section 5.2.5). Except for the central region, the composition is set as the solar metallicity. We use our standard  $B_q = 1$ .

Figure 14 shows the result of the numerical calculation. Overall, the parameters suggested by Chatzopoulos, Wheeler, & Vinko (2012) do not result in a similar LC to that of SN 2006gy. The peak luminosity of the bolometric LC is close to that of SN 2006gy but the duration is much shorter than that of SN 2006gy. In addition, the  $R$  band peak luminosity is much smaller than that of SN 2006gy because the photospheric temperature is much higher than that of SN 2006gy around the peak and the model has much bluer spectra. The duration can be longer if we use a smaller  $B_q$  but our results shown in Figure 11 imply that it is difficult to make the duration two times longer than the  $B_q = 1$  LC to match the LC of SN 2006gy by just making the  $B_q$  small. What is more, changing  $B_q$  does not improve the color of the LC and the  $R$  band LC is expected to remain much fainter than the observed  $R$  band LC. The plateau phase after the drop in the LC is due to the recombination in  $40 M_{\odot}$  SN ejecta inside. The duration of the plateau phase should actually be much shorter than that in Figure 14, as the entire SN ejecta is composed of the solar metallicity in the model (except for the central  $^{56}\text{Ni}$ ) and we use an approximate density structure for the SN ejecta.

There are several possible reasons for the discrepancy. The semi-analytic model assumes that the thermal energy gained by the forward shock is always released at the center of the CSM because the assumption is required to treat the transport equations analytically. However, this assumption keeps the diffusion time of the photons from the forward shock constant and the diffusion time is fixed with the initial value. In reality, the forward shock travels outward and the diffusion time decreases with time as the remaining unshocked wind decreases. This effect leads to the overestimation of the duration of the LCs in the semi-analytic model. This is presumed to be the main reason why the duration of the LC obtained by the numerical calculation is much

shorter than that obtained by the analytical model. This indicates that the semi-analytic model should not be applied to the system with CSM of a large initial diffusion time in which the kinetic energy of shock waves is the main source of radiation.

Another possible reason is that the energy released by the reverse shock is overestimated in the semi-analytic model. In the semi-analytic model, the self-similar solution of Chevalier (1982); Nadezhin (1985) is used as the evolution of the hydrodynamical structure. However, in reality, the effect of cooling which is not taken into account in the adiabatic self-similar solution is so strong in the case of SLSNe powered by the shock interaction that a thin cool dense shell is created between the SN ejecta and the dense CSM. Thus, the reverse shock could not travel as fast as expected from the adiabatic self-similar solution and rather stays close to the forward shock.

In summary, many important effects which are essential in modeling the LC powered by the shock interaction between SN ejecta and a dense CSM with a large photon diffusion time lack in the semi-analytic model and it may not be appropriate to use it for the modeling of SLSNe powered by such a strong interaction.

#### 6.5 High-Redshift Type II<sub>n</sub> Superluminous Supernovae

SLSNe powered by the shock interaction are not only brighter but also bluer than other SNe. Thus, SLSNe are expected to be a good probe to study the high-redshift Universe. Especially, as their progenitors are expected to be very massive (Section 6.3), SLSNe can provide us with the information of very massive stars in the early Universe. Some high-redshift Type II<sub>n</sub> SNe are already detected up to  $z = 2.36$  (Cooke et al. 2009, see also Barton & Cooke 2010).

With upcoming optical deep surveys with, e.g., Subaru/Hyper Suprime-Cam (HSC) (Miyazaki et al. 2006), SLSNe powered by the interaction can be detected up to  $z \sim 5$  (e.g., Tanaka et al. 2012; Cooke 2008) where as PISNe can be detected up to  $z \sim 2$  (e.g., Pan, Loeb, & Kasen 2012). Upcoming NIR surveys by, e.g., James Webb Space Telescope (JWST)<sup>1</sup>, Euclid<sup>2</sup>, or Wide-field Imaging Surveyor for High-redshift (WISH)<sup>3</sup>, can approach to much higher redshifts (e.g., Tanaka et al. 2012; Pan, Kasen, & Loeb 2012; Hummel et al. 2011; Scannapieco et al. 2005). Here, we show how the LC of SN 2006gy is observed if it appears at high redshifts. This can be used for the identification of candidate transients obtained in upcoming optical and NIR surveys.

Figure 15 is the  $i$  band LCs of the model D2 ( $w = 5$ ) and F1 ( $w = 0$ ) for several redshifts. As the model F1 has similar color to SN 2006gy at around the LC peak, the F1 model provides better estimate for the high-redshift SLSN LCs. Figure 16 is the LCs with the F277W filter<sup>4</sup> which is one of the wide filters planned for JWST. The central wavelength of the F277W filter is at  $2.77 \mu\text{m}$ . JWST can

<sup>1</sup> <http://www.jwst.nasa.gov/>

<sup>2</sup> <http://sci.esa.int/euclid>

<sup>3</sup> <http://www.wishmission.org/en/index.html>

<sup>4</sup> <http://www.stsci.edu/jwst/instruments/nircam/instrumentdesign/filters/>



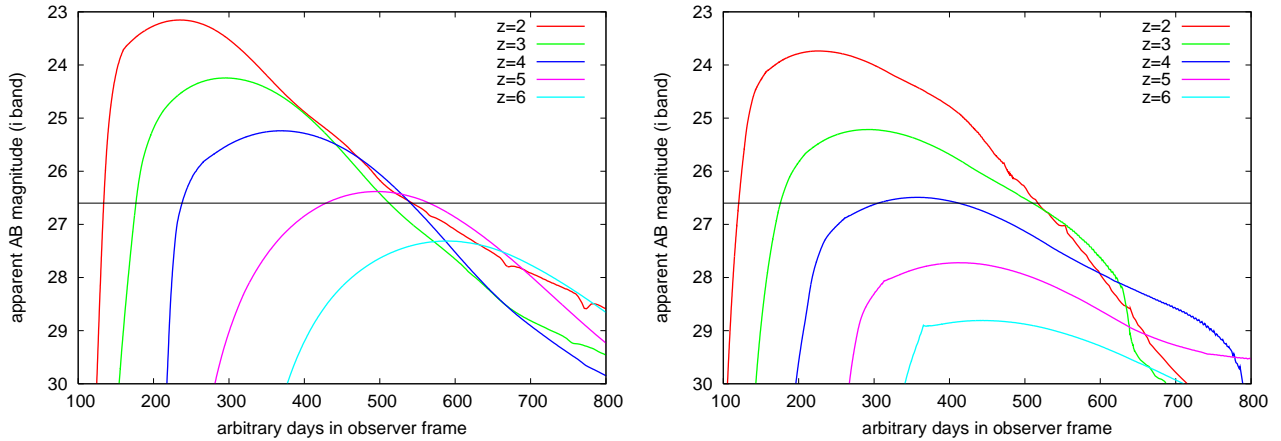


**Figure 15.** *i* band LCs of the models D2 ( $w = 5$ , left) and F1 ( $w = 0$ , right) at several redshifts. The horizontal line is the planned *i* band limiting magnitude of Subaru/HSC Ultra-Deep survey at one epoch (26.6 mag).

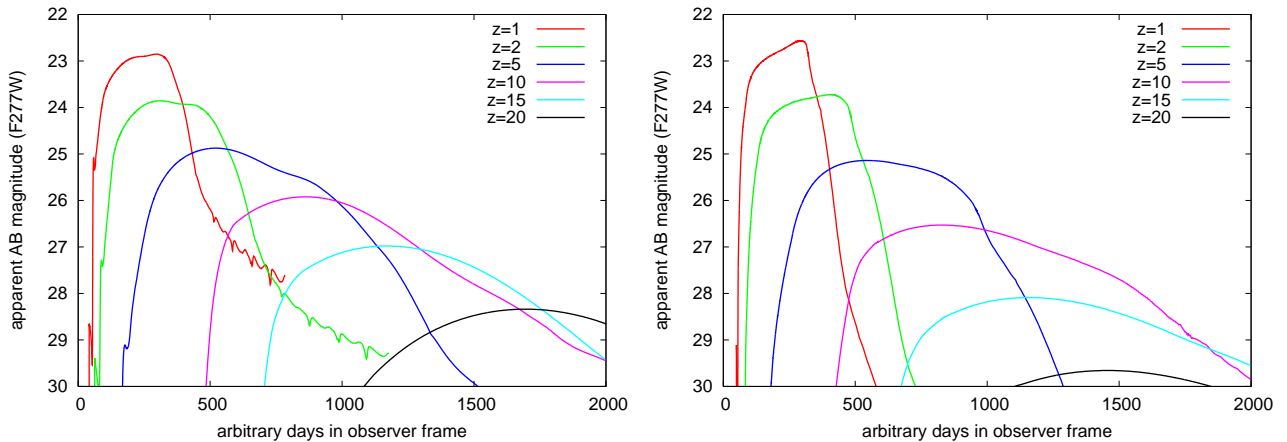


**Figure 16.** F277W band LCs of the models D2 ( $w = 5$ , left) and F1 ( $w = 0$ , right) at several redshifts.

reach  $\simeq 30$  mag and is able to detect SLSNe beyond  $z = 10$ . See Tanaka et al. (2012) for the details of observational strategies and estimated number of detections of SLSNe with upcoming optical and NIR surveys.

## 7 SUMMARY AND CONCLUSIONS

We have shown that the interaction between SN ejecta and dense CSM is a viable mechanism to power SLSNe such as SN 2006gy. The interaction in the dense CSM accounts for the huge luminosity and the long duration of the SN 2006gy LC. Shock breakout within the dense CSM is a key for the understanding of the interaction-powered SLSNe. Our canonical models have  $M_{\text{ej}} = 20 M_{\odot}$ ,  $E_{\text{ej}} = 10^{52}$  erg, and  $M_{\text{CSM}} = 18 M_{\odot}$  ( $w = 5$ ) or  $15 M_{\odot}$  ( $w = 0$ ) where the CSM is assumed to have a density profile of  $\rho \propto r^{-w}$ . The corresponding average mass-loss rate of the progenitor is about  $0.4 M_{\odot} \text{ yr}^{-1}$  if we assume that the dense CSM originates from a  $100 \text{ km s}^{-1}$  wind. Our steady mass-loss models ( $w = 2$ ) fail to explain the SN 2006gy LC. No  $^{56}\text{Ni}$  is required to explain the early LC of SN 2006gy.

It is difficult to break the degeneracy among  $M_{\text{ej}}$ ,  $E_{\text{ej}}$ ,

and  $M_{\text{CSM}}$ . One can obtain constraints on the progenitor of SN 2006gy based on the efficiency, as the conversion efficiency of the SN kinetic energy to radiation becomes high when  $M_{\text{ej}}$  is comparable to or less than  $M_{\text{CSM}}$ . The progenitor of SN 2006gy should be a very massive star because  $M_{\text{CSM}} = 18 M_{\odot}$  or  $15 M_{\odot}$ . As the conversion efficiency is  $\simeq 50\%$  at most and the radiation energy emitted by SN 2006gy is more than  $2 \times 10^{51}$  erg,  $E_{\text{ej}}$  should be larger than  $4 \times 10^{51}$  erg.

We have also examined the effect of multidimensional instabilities in the dense cool shell on the model LCs. Such instabilities are expected to reduce the amount of kinetic energy converted to radiation. Our LC modeling is based on a one-dimensional radiation hydrodynamics code in which the multidimensional instabilities are implemented only in an approximate way. We have thus explore the effect qualitatively. Further studies on the multidimensional effect(s), perhaps using three-dimensional radiation hydrodynamics simulations, are needed for better understanding of SNe powered by the interaction.

Finally, we have provided predictions from our model for high-redshift SLSNe. We have calculated the optical and



NIR LC evolution in the observer frame. The results can be used for the identification of SLSNe appeared at high redshifts in the future transient surveys.

The existence of the very massive CSM close to the progenitor which is required to explain the LC of SN 2006gy challenges the current understanding of the stellar mass loss. The better understanding of SNe powered by the interaction will lead us to the better understanding of the mass loss mechanisms of massive stars. This is a critical key to reveal the evolution and the fates of massive stars which are a fundamental component in the Universe.

## ACKNOWLEDGMENTS

We thank the anonymous referee for the comments. T.J.M. is supported by the Japan Society for the Promotion of Science Research Fellowship for Young Scientists (23 · 5929). S.I.B. is supported partly by the grants of the Government of the Russian Federation (No 11.G34.31.0047), RFBR 10-02-00249, 10-02-01398, by RF Sci. Schools 3458.2010.2 and 3899.2010.2, and by a grant IZ73Z0-128180/1 of the Swiss National Science Foundation (SCOPES). All the numerical calculations were carried out on the general-purpose PC farm at Center for Computational Astrophysics, CfCA, of National Astronomical Observatory of Japan. N.Y. acknowledges support by the Grants-in-Aid for Young Scientists (S: 20674003) by the Japan Society for the Promotion of Science. This research is supported in part by a grant from the Hayakawa Satio Fund awarded by the Astronomical Society of Japan. This research is also supported by World Premier International Research Center Initiative, MEXT, Japan.

## APPENDIX A: EFFECT OF THE SMEARING TERM ON LIGHT CURVES OF PULSATONAL PAIR-INSTABILITY SUPERNOVAE

We show the results of our additional investigations on the dependence of the smearing term  $B_q$  on the results of LC calculations. We show the results obtained from the pulsational-pair instability SN models presented by Woosley, Blinnikov, & Heger (2007) and show that the effect of  $B_q$  on LCs is similar to our LC models. This means that the effect of  $B_q$  appeared in our models is not unique to our models.

The models presented here are based on the same progenitor model ( $M_{ZAMS} = 110 M_{\odot}$ ) shown in Woosley, Blinnikov, & Heger (2007). The shell ejected by the first pulsation ( $24.5 M_{\odot}$ ) is caught up by the materials ejected by the next pulsation ( $5.1 M_{\odot}$ ). Woosley, Blinnikov, & Heger (2007) have artificially increased the kinetic energy of the materials ejected by the second pulsation to obtain the better fit to the LC of SN 2006gy and their best LC model has four times as much kinetic energy as that of the original model. The models shown here have more kinetic energy. The kinetic energy of the second pulse is increased nine times and the kinetic energy of the second pulse is  $6.5 \times 10^{51}$  erg. The rest of the model is the same as those discussed in Woosley, Blinnikov, & Heger (2007).

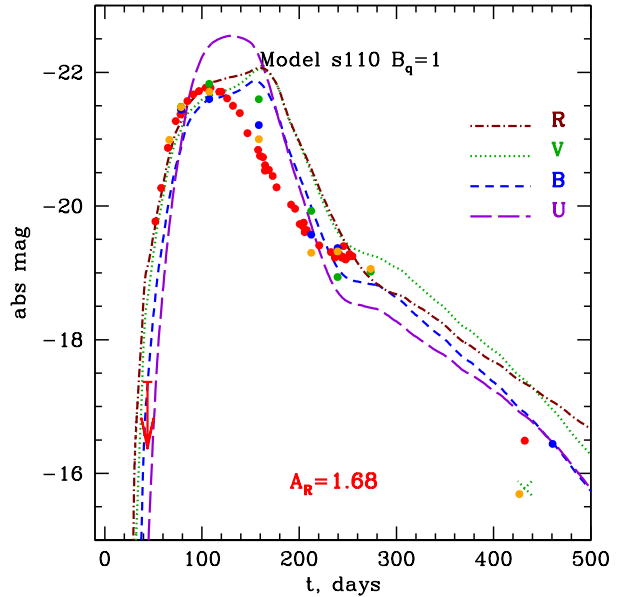


**Figure A1.** LCs of a pulsational-pair instability model with  $B_q = 1$ . The kinetic energy of the second pulse is increased nine times as large as the original model. Note that slightly higher absorption ( $A_R = 1.68$  mag) is applied in the observational data points than the value adopted in the other part of this paper ( $A_R = 1.3$  mag).

Figures A1, A2, and A3 show the results of the LC calculations with different  $B_q$ . Comparing the results to those shown in Figure 11, we can see that the dependence of the results on  $B_q$  is basically the same. This is because the source of the luminosity in both the models is kinetic energy of the material coming from inside and  $B_q$  directly affects the conversion efficiency of the kinetic energy to the radiation energy. For the accurate modeling of the LCs resulting from the conversion of the kinetic energy to radiation, we need more investigations on the multidimensional effects during the interaction.

## REFERENCES

- Agnoletto I., et al., 2009, *ApJ*, 691, 1348
- Arcavi I., et al., 2010, *ApJ*, 721, 777
- Argo M. K., Beswick R. J., Muxlow T. W. B., Pedlar A., 2007, *ATel*, 1084, 1
- Arnett W. D., Meakin C., 2011, *ApJ*, 741, 33
- Baklanov P. V., Blinnikov S. I., Pavlyuk N. N., 2005, *AstL*, 31, 429
- Balberg S., Loeb A., 2011, *MNRAS*, 414, 1715
- Barbary K., et al., 2009, *ApJ*, 690, 1358
- Barkat Z., Rakavy G., Sack N., 1967, *PhRvL*, 18, 379
- Barton E. J., Cooke J., 2010, *AIPC*, 1294, 196
- Berger E., et al., 2012, *arXiv*, arXiv:1206.4050
- Benvenuto O. G., Lugones G., 1999, *MNRAS*, 304, L25
- Bietenholz M., Bartel N., 2007, *ATel*, 1254, 1
- Bietenholz M., Bartel N., 2008a, *ATel*, 1525, 1
- Bietenholz M., Bartel N., 2008b, *ATel*, 1657, 1
- Blinnikov S. I., 2008, *AIPC*, 1016, 241

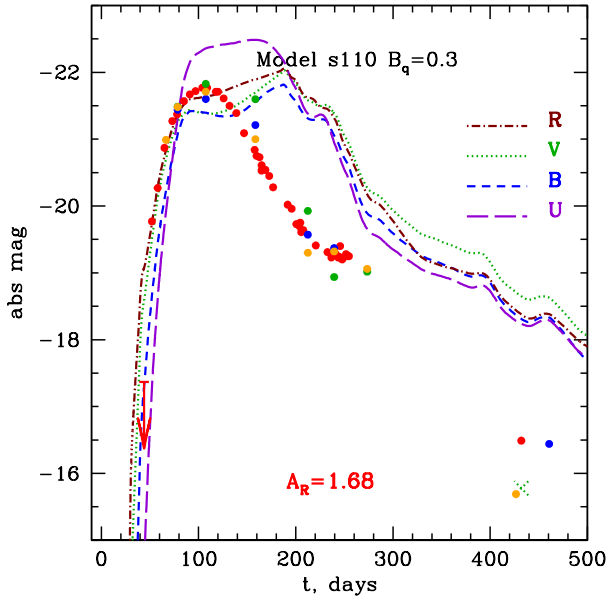


Figure A2. The same as Figure A1 but  $B_q = 0.3$ .

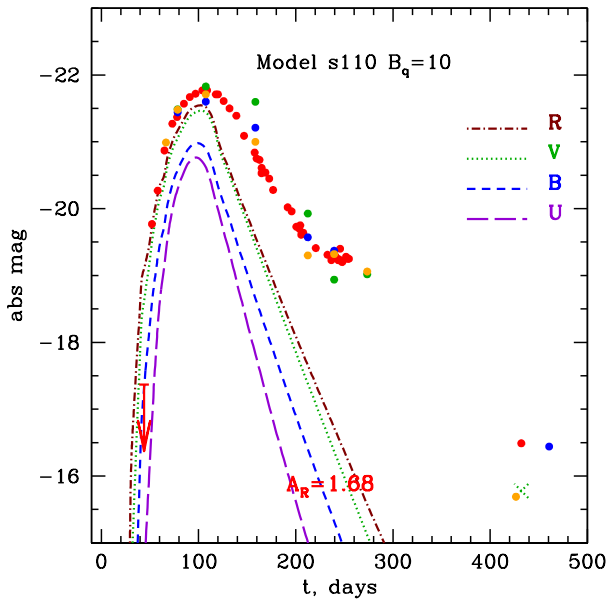


Figure A3. The same as Figure A1 but  $B_q = 10$ .

Blinnikov S. I., Bartunov O. S., 1993, *A&A*, 273, 106  
 Blinnikov S., Chugai N., Lundqvist P., Nadyozhin D.,  
 Woosley S., Sorokina E., 2003, *ftp.conf*, 23  
 Blinnikov S. I., Eastman R., Bartunov O. S., Popolitov  
 V. A., Woosley S. E., 1998, *ApJ*, 496, 454  
 Blinnikov S., Lundqvist P., Bartunov O., Nomoto K.,  
 Iwamoto K., 2000, *ApJ*, 532, 1132  
 Blinnikov S. I., Röpke F. K., Sorokina E. I., Gieseler M.,  
 Reinecke M., Travaglio C., Hillebrandt W., Stritzinger M.,  
 2006, *A&A*, 453, 229

Blinnikov S. I., Sorokina E. I., 2010, arXiv, arXiv:1009.4353  
 Blinnikov S. I., Tolstov A. G., 2011, *AstL*, 37, 194  
 Boyer M. L., et al., 2010, *A&A*, 518, L142  
 Cardelli J. A., Clayton G. C., Mathis J. S., 1989, *ApJ*, 345,  
 245  
 Chandra P., Chakraborti S., Ray A., 2007, *ATel*, 1082, 1  
 Chatzopoulos E., Wheeler J. C., Vinko J., 2012, *ApJ*, 746,  
 121  
 Chatzopoulos E., et al., 2011, *ApJ*, 729, 143  
 Chevalier R. A., 1982, *ApJ*, 258, 790  
 Chevalier R. A., 2012, *ApJ*, 752, L2  
 Chevalier R., Blondin J. M., 1995, *ApJ*, 444, 312  
 Chevalier R. A., Fransson C., 1994, *ApJ*, 420, 268  
 Chevalier R. A., Irwin C. M., 2011, *ApJ*, 729, L6  
 Chevalier R. A., Irwin C. M., 2012, *ApJ*, 747, L17  
 Chevalier R. A., Soker N., 1989, *ApJ*, 341, 867  
 Chomiuk L., et al., 2011, *ApJ*, 743, 114  
 Chugai N. N., 2001, *MNRAS*, 326, 1448  
 Chugai N. N., et al., 2004, *MNRAS*, 352, 1213  
 Cooke J., 2008, *ApJ*, 677, 137  
 Cooke J., Sullivan M., Barton E. J., Bullock J. S., Carlberg  
 R. G., Gal-Yam A., Tollerud E., 2009, *Natur*, 460, 237  
 Crowther P. A., 2007, *ARA&A*, 45, 177  
 Deng J., et al., 2004, *ApJ*, 605, L37  
 Dessart L., Hillier D. J., Gezari S., Basa S., Matheson T.,  
 2009, *MNRAS*, 394, 21  
 Drake A. J., et al., 2009, *ApJ*, 696, 870  
 Drake A. J., et al., 2010, *ApJ*, 718, L127  
 Drake A. J., et al., 2011, *ApJ*, 735, 106  
 Dwarkadas V. V., 2011, *MNRAS*, 412, 1639  
 Dwarkadas V. V., Gruszko J., 2011, *MNRAS*, 1782  
 Filippenko A. V., 1997, *ARA&A*, 35, 309  
 Folatelli G., et al., 2006, *ApJ*, 641, 1039  
 Gal-Yam A., Leonard D. C., 2009, *Natur*, 458, 865  
 Gal-Yam A., et al., 2007, *ApJ*, 656, 372  
 Gal-Yam A., et al., 2009, *Natur*, 462, 624  
 Georgy C., 2012, *A&A*, 538, L8  
 Gezari S., et al., 2009, *ApJ*, 690, 1313  
 Ginzburg S., Balberg S., 2012, arXiv, arXiv:1205.3455  
 Hachisu I., Kato M., Nomoto K., 2008, *ApJ*, 679, 1390  
 Hamuy M., et al., 2003, *Natur*, 424, 651  
 Heger A., Jeannin L., Langer N., Baraffe I., 1997, *A&A*,  
 327, 224  
 Hodapp K. W., et al., 2004, *AN*, 325, 636  
 Hummel J., Pawlik A., Milosavljevic M., Bromm V., 2011,  
 arXiv, arXiv:1112.5207  
 Humphreys R. M., Davidson K., 1994, *PASP*, 106, 1025  
 Kasen D., Bildsten L., 2010, *ApJ*, 717, 245  
 Kasen D., Woosley S. E., 2009, *ApJ*, 703, 2205  
 Kasen D., Woosley S. E., Heger A., 2011, *ApJ*, 734, 102  
 Kawabata K. S., Tanaka M., Maeda K., Hattori T., Nomoto  
 K., Tominaga N., Yamanaka M., 2009, *ApJ*, 697, 747  
 Kiewe M., et al., 2012, *ApJ*, 744, 10  
 Kostka M., Koning N., Ouyed R., Leahy D., Steffen W.,  
 2012, arXiv, arXiv:1206.7113  
 Kotak R., Vink J. S., 2006, *A&A*, 460, L5  
 Law N. M., et al., 2009, *PASP*, 121, 1395  
 Leahy D., Ouyed R., 2008, *MNRAS*, 387, 1193  
 Leloudas G., et al., 2012, *A&A*, 541, A129  
 Li Y., Gong Z. G., 1994, *A&A*, 289, 449  
 Maeda K., et al., 2007, *ApJ*, 666, 1069

- Miller A. A., Smith N., Li W., Bloom J. S., Chornock R., Filippenko A. V., Prochaska J. X., 2010, *AJ*, 139, 2218
- Miller A. A., et al., 2009, *ApJ*, 690, 1303
- Miyazaki S., et al., 2006, *SPIE*, 6269,
- Modjaz M., Kewley L., Bloom J. S., Filippenko A. V., Perley D., Silverman J. M., 2011, *ApJ*, 731, L4
- Moriya T. J., Tominaga N., 2012, *ApJ*, 747, 118
- Moriya T., Tominaga N., Blinnikov S. I., Baklanov P. V., Sorokina E. I., 2011, *MNRAS*, 415, 199
- Moriya T., Tominaga N., Tanaka M., Maeda K., Nomoto K., 2010, *ApJ*, 717, L83
- Nadezhin D. K., 1985, *Ap&SS*, 112, 225
- Nakar E., Sari R., 2010, *ApJ*, 725, 904
- Nomoto K., Maeda K., Tanaka M., Suzuki T., 2011, *Ap&SS*, 336, 129
- Nomoto K., Tominaga N., Tanaka M., Maeda K., Umeda H., 2007, *AIPC*, 937, 412
- Ofek E. O., et al., 2010, *ApJ*, 724, 1396
- Ofek E. O., et al., 2007, *ApJ*, 659, L13
- Ohkubo T., Nomoto K., Umeda H., Yoshida N., Tsuruta S., 2009, *ApJ*, 706, 1184
- Ouyed R., Kostka M., Koning N., Leahy D. A., Steffen W., 2012, *MNRAS*, 423, 1652
- Pan T., Kasen D., Loeb A., 2012, *MNRAS*, 422, 2701
- Pan T., Loeb A., Kasen D., 2012, *MNRAS*, 2979
- Pastorello A., et al., 2010, *ApJ*, 724, L16
- Portegies Zwart S. F., van den Heuvel E. P. J., 2007, *Natur*, 450, 388
- Quataert E., Shiode J., 2012, *MNRAS*, 423, L92
- Quimby R. M., 2006a, PhD, University of Texas
- Quimby R., 2006b, *CBET*, 644, 1
- Quimby R. M., Aldering G., Wheeler J. C., Höflich P., Akserlof C. W., Rykoff E. S., 2007, *ApJ*, 668, L99
- Quimby R. M., et al., 2011, *Natur*, 474, 487
- Rabinak I., Waxman E., 2011, *ApJ*, 728, 63
- Rakavy G., Shaviv G., 1967, *ApJ*, 148, 803
- Rau A., et al., 2009, *PASP*, 121, 1334
- Rest A., et al., 2011, *ApJ*, 729, 88
- Sanders N. E., et al., 2012, *arXiv*, arXiv:1206.2643
- Scannapieco E., Madau P., Woosley S., Heger A., Ferrara A., 2005, *ApJ*, 633, 1031
- Schlegel D. J., Finkbeiner D. P., Davis M., 1998, *ApJ*, 500, 525
- Schlegel E. M., 1990, *MNRAS*, 244, 269
- Smith N., Hinkle K. H., Ryde N., 2009, *AJ*, 137, 3558
- Smith N., Chornock R., Silverman J. M., Filippenko A. V., Foley R. J., 2010, *ApJ*, 709, 856
- Smith N., McCray R., 2007, *ApJ*, 671, L17
- Smith N., Owocki S. P., 2006, *ApJ*, 645, L45
- Smith N., et al., 2007, *ApJ*, 666, 1116
- Smith N., et al., 2008, *ApJ*, 686, 485
- Smith N., et al., 2011, *ApJ*, 732, 63
- Soker N., 2012, *arXiv*, arXiv:1204.3173
- Svirski G., Nakar E., Sari R., 2012, *arXiv*, arXiv:1202.3437
- Tanaka M., Moriya T. J., Yoshida N., Nomoto K., 2012, *MNRAS*, 422, 2675
- Tominaga N., Morokuma T., Blinnikov S. I., Baklanov P., Sorokina E. I., Nomoto K., 2011, *ApJS*, 193, 20
- Trundle C., Kotak R., Vink J. S., Meikle W. P. S., 2008, *A&A*, 483, L47
- Tsvetkov D. Y., Volkov I. M., Baklanov P., Blinnikov S., Tuchin O., 2009, *PZ*, 29, 2
- Umeda H., Nomoto K., 2008, *ApJ*, 673, 1014
- Vanbeveren D., Van Bever J., Belkus H., 2007, *ApJ*, 662, L107
- van Loon J. T., Cioni M.-R. L., Zijlstra A. A., Loup C., 2005, *A&A*, 438, 273
- van Marle A. J., Smith N., Owocki S. P., van Veelen B., 2010, *MNRAS*, 407, 2305
- Vink J. S., 2009, *arXiv*, arXiv:0905.3338
- Weaver T. A., 1976, *ApJS*, 32, 233
- Woosley S. E., 2010, *ApJ*, 719, L204
- Woosley S. E., Blinnikov S., Heger A., 2007, *Natur*, 450, 390
- Woosley S. E., Kasen D., Blinnikov S., Sorokina E., 2007, *ApJ*, 662, 487
- Yoon S.-C., Cantiello M., 2010, *ApJ*, 717, L62